NASA CONTRACTOR REPORT

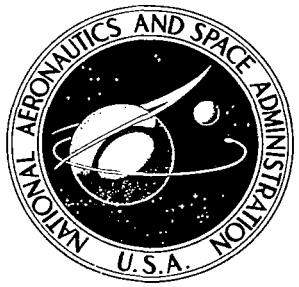

THE REFLECTION COEFFICIENT OF A TEM MODE PARALLEL-PLATE WAVEGUIDE ILLUMINATING A CONDUCTING SHEET: THE LARGE WEDGE ANGLE CASE

by W. D. Burnside, L. L. Tsai, and R. C. Rudduck

Prepared by
OHIO STATE UNIVERSITY
Columbus, Ohio
for

NATIONAL AERONAUTICS AND SPACE ADMINISTRATION • WASHINGTON, D. C. • SEPTEMBER 1968

NASA CR-1174

THE REFLECTION COEFFICIENT OF A TEM MODE PARALLEL-PLATE WAVEGUIDE ILLUMINATING A CONDUCTING SHEET: THE LARGE WEDGE ANGLE CASE

By W. D. Burnside, L. L. Tsai, and R. C. Rudduck

Prepared under Grant No. NGR-36-008-048 by
OHIO STATE UNIVERSITY
Columbus, Ohio

for

NATIONAL AERONAUTICS AND SPACE ADMINISTRATION

For sale by the Clearinghouse for Federal Scientific and Technical Information
Springfield, Virginia 22151 – CFSTI price $3.00

ABSTRACT

The reflection coefficient of a large wedge angle parallel-plate waveguide operating in the TEM mode and illuminating a perfectly conducting sheet is analyzed by wedge diffraction techniques. The interactions between the waveguide aperture and the reflector are represented by bouncing cylindrical waves. The scattering of these cylindrical waves by the guide aperture produces four subsequent component cylindrical waves, which in turn reflect back onto the guide. These component cylindrical waves are determined through analysis and are represented by equivalent line sources which then couple power into the guide. The continuation of this reiteration process then includes the contribution of the higher-order interactions (or bounces). Good agreement is obtained between the calculated results and measurements. The calculated results also agree with those obtained by the plane-wave approach of Reference 1, Chapter IV in the region of mutual validity for both analyses.

TABLE OF CONTENTS

		Page
I.	INTRODUCTION	1
	A. Statement of the Problem	1
	B. Background	2
	C. First-Bounce Wave	3
II.	BACKSCATTERING MECHANISM OF THE WAVEGUIDE WITH AN INCIDENT CYLINDRICAL WAVE	5
	A. Actual Guide Backscattering	5
	B. Representation of Solid Wedge Scattering by Cylindrical Wave Components	10
	Case I	15
	Case II	19
	C. Aperture Component of the Scattered Field	20
III.	REFLECTION COEFFICIENT ANALYSIS	21
IV.	RESULTS	25
V.	CONCLUSIONS	41
REFERENCES		42

THE REFLECTION COEFFICIENT OF A TEM MODE PARALLEL-PLATE WAVEGUIDE ILLUMINATING A CONDUCTING SHEET: THE LARGE WEDGE ANGLE CASE

I. INTRODUCTION

A. Statement of the Problem

Wedge diffraction theory is used in this analysis to calculate the reflection coefficient of a TEM mode, symmetric, parallel-plate waveguide with large wedge angles and illuminating a perfectly reflecting sheet. The general geometry of the problem to be considered is shown in Fig. 1.

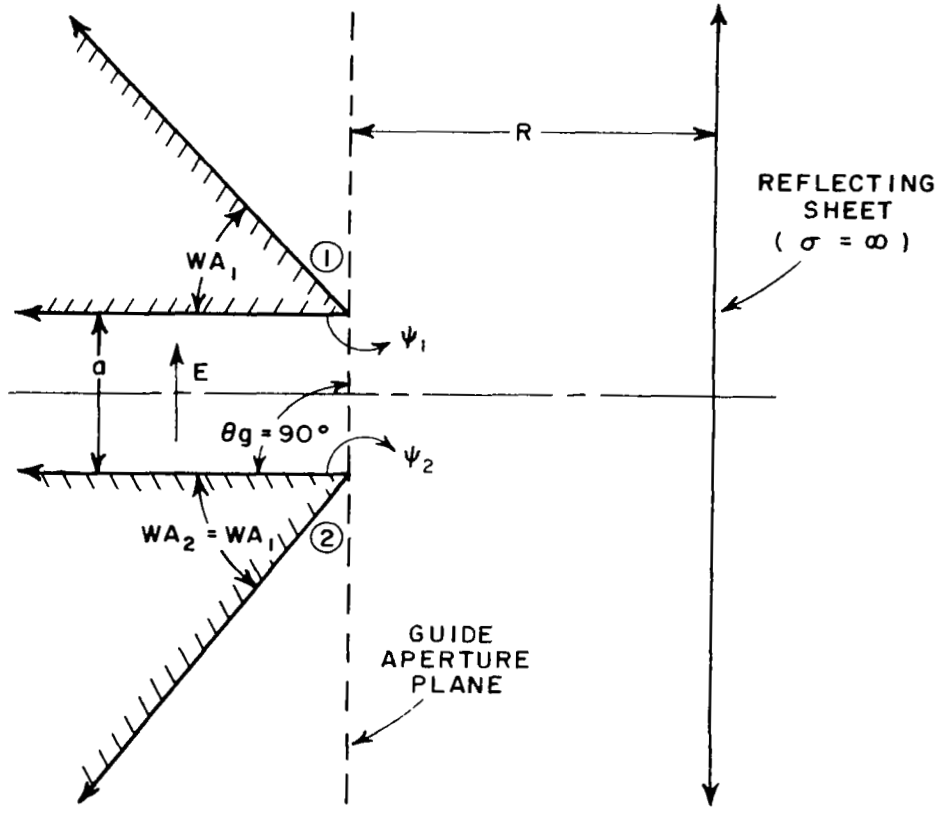

Fig. 1. Parallel-plate waveguide illuminating a reflecting sheet.

Analysis of this reflecting-sheet problem gives insight into the basic diffraction behavior of small aperture antennas which radiate into over-dense plasmas. The analysis is applicable for spacecraft reentry situations in which the plasma medium can be adequately modeled by a simple reflecting sheet.

The same problem with small wedge angles (less than 70°) has been formulated using plane waves to describe the interactions between the waveguide and the reflector.[1] The ground-plane mounted guide was analyzed by successively bouncing cylindrical waves.[1,2] For that case only two component cylindrical waves result from the scattering of an incident cylindrical wave by the ground plane with a waveguide aperture. In this report a similar superposition technique will be used to describe the scattering by the waveguide wedges for guides with large wedge angles (70°-90°). However, four cylindrical wave components result in this case.

B. Background

The incident TEM mode within the parallel-plate waveguide propagates as shown in Fig. 1 and is assumed to have a unit amplitude magnetic field parallel to the guide walls. Integration of the Poynting vector, which is uniform across the guide, over the guide cross section yields the power flow per unit depth of the guide as $(Z_o a)$, where Z_o is the free-space impedance and (a) is the width of the guide. The modal current is then given by

$$I_o = \sqrt{a} \tag{1}$$

Equivalent line sources with omni-directional patterns are employed in the subsequent analyses. The modal current I of an isotropic line source is related to its radiated magnetic field H, diffraction coefficient D, and ray R by

$$H = I\frac{e^{-jkr + j\frac{\pi}{4}}}{\sqrt{2\pi r}} = \frac{e^{-j\left(kr + \frac{\pi}{4}\right)}}{\sqrt{2\pi kr}} R = \frac{e^{-jkr}}{\sqrt{r}} D \tag{2}$$

The response of a guide to an equivalent line source is obtained through reciprocity and given in terms of modal current ratio as[3,4]

$$(3) \qquad \frac{I_R}{I_T} = \sqrt{\frac{\lambda}{2\pi a}}\, H_T(r,\theta)$$

where I_T is the modal current of the transmitting line source, I_R is the receiving guide modal current, and $H_T(r,\theta)$ is the field of the guide at the line source location when the guide is transmitting with a modal current $I_o = \sqrt{a}$.

The free-space reflection coefficient, Γ_s, of the waveguide (that is, with the guide radiating into free space) is given by[5]

$$(4) \qquad \Gamma_s = \frac{I}{I_o} = \frac{1}{2}\frac{\sqrt{\lambda}}{a}\left[D_1(\psi_1 = 0) + D_2(\psi_2 = 0)\right] e^{-j\frac{\pi}{4}} \quad ,$$

where $D_1(\psi_1 = 0)$ and $D_2(\psi_2 = 0)$ are the total diffraction coefficients for edges 1 and 2 corresponding to the rays diffracted back along the inside of the waveguide walls.

C. First-Bounce Wave

The near-zone fields of a guide in free space may be computed as discussed in Reference 1, Section IIA, by including the geometrical optics, and the singly diffracted and the doubly diffracted contributions. Calculations of the field distribution of the parallel-plate waveguide obtained by the above method indicate that the radiation from the guide in the vicinity of the projected guide aperture may be treated as that of a cylindrical wave with its source at the center of the aperture. This free-space wave, calculated at a distance (2R) from the aperture, represents the reflected wave incident on the guide aperture coming from the conducting sheet, located at a distance (R) from the aperture. This reflected wave is called the first-bounce wave.

Because the first-bounce wave is cylindrical, an equivalent line source located at a distance (2R) on the guide axis may be introduced to compute the first-bounce contribution to the reflection coefficient by using the line source to waveguide coupling expression of Eq. (3). The modal current of this equivalent line source is related to the first-bounce magnetic field at the center of the guide aperture by Eq. (2) and is given by

$$(5) \qquad I_{eq}^{(1)} = \sqrt{2\pi(2R)}\; e^{+jk(2R) - j\frac{\pi}{4}}\; H_T \quad ,$$

where H_T is the free-space magnetic field radiated by the guide at a distance (2R) along the guide axis as computed by the method in Reference 1. Line source to waveguide coupling then yields the modal current induced in the guide by the first-bounce wave as

$$(6) \qquad I_R^{(1)} = I_{eq}^{(1)} \sqrt{\frac{\lambda}{2\pi a}} \; H_T$$

The contribution to the reflection coefficient by the first-bounce wave is thus given by

$$(7) \qquad \Gamma^{(1)} = \frac{I_R^{(1)}}{I_o} = \frac{I_R^{(1)}}{\sqrt{a}}$$

$$= \frac{I_{eq}^{(1)}}{a} \sqrt{\frac{\lambda}{2\pi}} \; H_T$$

For the ground-plane mounted guide[1,2] the scattering of the first-bounce wave by the guide aperture causes a second-bounce wave composed of two component cylindrical waves. As shown in Fig. 2 the second-bounce wave is composed of the reflected geometrical optics field from a ground plane and the aperture component which is very similar to the scattered wave from a rectangular wall.

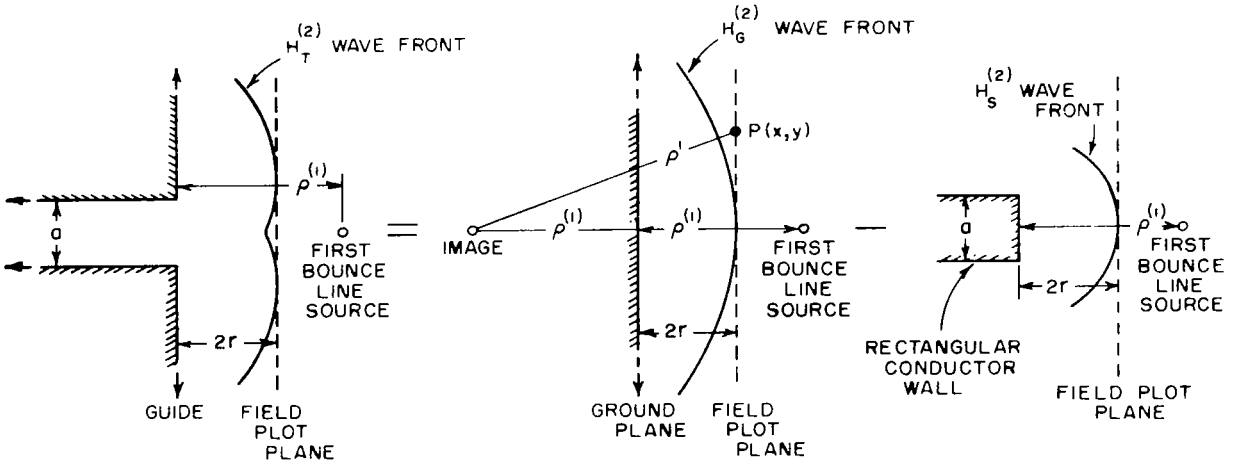

Fig. 2. Application of superposition to line source field diffraction by a ground-plane guide aperture.

For the large wedge angle case (70°-90°) considered in this report, the waveguide scattering mechanism with an incident cylindrical wave causes four subsequent component cylindrical waves, as will be discussed in the following sections.

II. BACKSCATTERING MECHANISM OF THE WAVEGUIDE WITH AN INCIDENT CYLINDRICAL WAVE

A. Actual Guide Backscattering

In order to calculate the higher-order interactions between the waveguide and the reflecting sheet it is necessary to analyze the back-scattered field from a line source illuminating the guide. As discussed in Section I, the free space radiation of the guide is reflected by the conducting sheet back onto the guide as a first-order interaction or bounce. The backscattering of the first-bounce wave from the waveguide gives rise to a second-bounce wave which reflects from the conducting sheet back onto the guide. This process continues, leading to higher-order inter-actions.

Each bounce wave or interaction can be treated as a superposition of cylindrical waves. Consequently, the succeeding bounce wave can be analyzed as the superposition of the scattered waves from each cylindrical wave component. In this section the scattering of an incident cylindrical wave by the waveguide wedges will be analyzed. As shown in Fig. 3 the guide is illuminated by the cylindrical wave from a line source located at radius ρ. The scattered wave which reflects from the sheet back onto the guide is the scattered wave incident on the image guide as shown in Fig. 3. For this reason the fields will be calculated in the plane normal to the guide axis at 2R from the guide, where R is the distance from the waveguide aperture to the reflecting sheet. Because of the symmetry of the problem involved, as shown in Fig. 3, only the upper half-space ($x = 2R$, $y \geq -a/2$) will be used throughout this analysis. The field value at an arbitrary observation point ($x = 2R$, y) is calculated by adding the geometrical optics, single diffraction, and double diffraction components.

The geometrical optics component of the scattered field is analyzed in terms of the image of the illuminating line source in the upper wedge. In terms of the coordinates (x, y) referred to edge ① of the waveguide, the image line source is located at (x', y'), as shown in Fig. 4. Let y_{min} be the vertical distance to the reflected field shadow boundary in

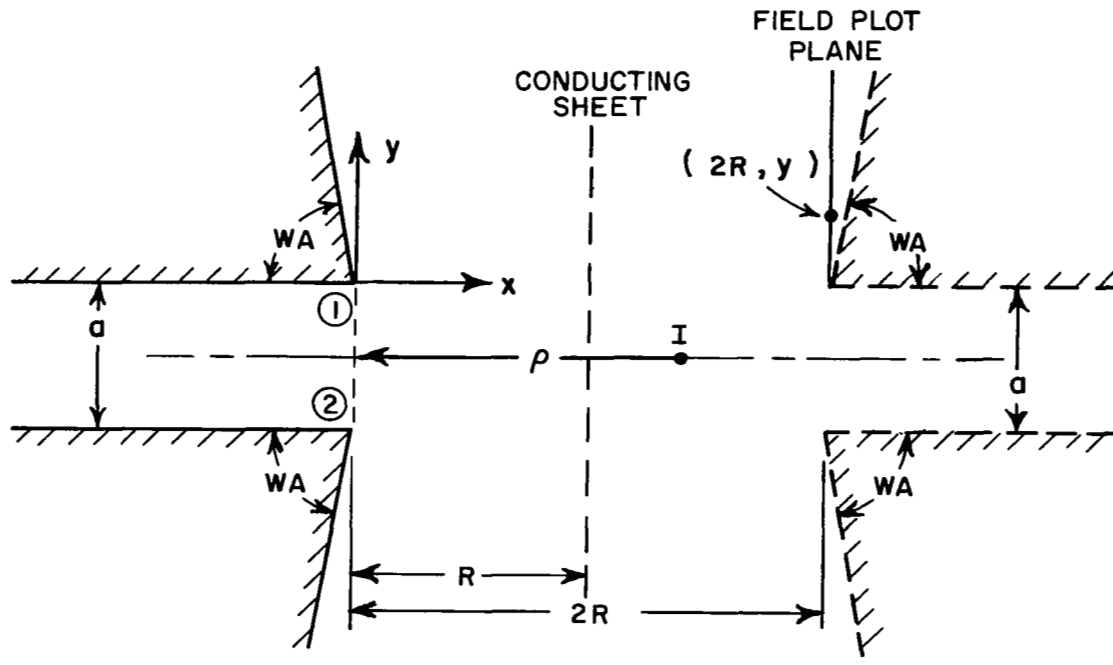

Fig. 3. Cylindrical wave backscattering geometry.

the plane of observation (x = 2R). Then the geometrical optics field component $[H_{GO}(2R, y)]$ is given as

$$(8) \qquad H_{GO}(2R, y) = \begin{cases} \dfrac{Ie^{-jkr_i + j\frac{\pi}{4}}}{\sqrt{2\pi r_i}} & y > y_{min} \\ 0 & y \leq y_{min} \end{cases} ,$$

where r_i is the distance from the image line source to the point of observation (2R, y) and is given by

$$(9) \qquad r_i = \sqrt{(x' + 2R)^2 + (y - y')^2} \quad .$$

The near-zone formulation for cylindrical wave diffraction as given in References 3 and 4 is used to determine the singly diffracted components of the field at (2R, y). The geometry for the analysis of these components is shown in Fig. 5. The single diffracted field from edge ① $[H_1^{(1)}(2R, y)]$ is given by

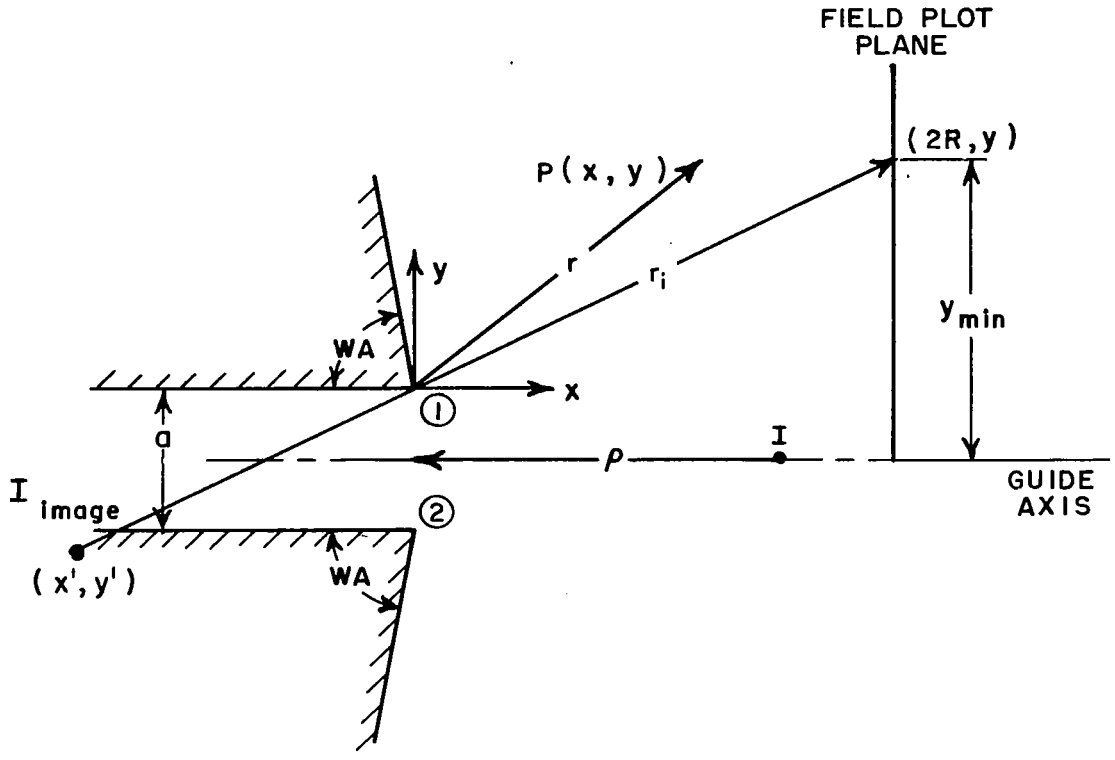

Fig. 4. Backscattering field plot geometry - the geometrical optics component.

$$H_1^{(1)}(2R, y) = U_1^{(1)} \times D_i \quad , \tag{10}$$

where

$$U_1^{(1)} = \frac{e^{-jk\left(r_1 + r_o - \frac{r_1 r_o}{r_1 + r_o}\right)}}{\sqrt{r_1 + r_o}} \left[V_B\left(\frac{r_1 r_o}{r_1 + r_o}, \theta_1 + \alpha\right) + V_B\left(\frac{r_1 r_o}{r_1 + r_o}, 2\pi + \theta_1 - \alpha\right)\right] \tag{11}$$

and

$$D_i = \frac{I e^{j\frac{\pi}{4}}}{\sqrt{2\pi}} \tag{12}$$

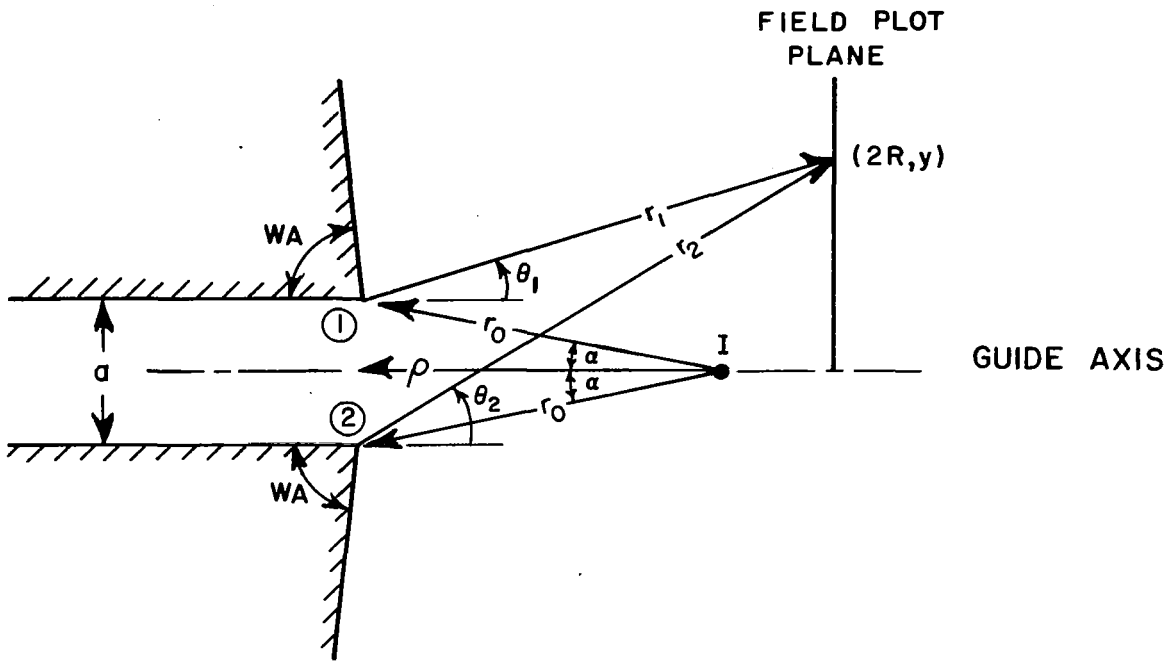

Fig. 5. Backscattering field plot geometry-the single diffraction component.

Therefore,

$$(13)\qquad H_1^{(1)}(2R,y) = \frac{I e^{j\frac{\pi}{4}}}{\sqrt{2\pi}} \quad \frac{e^{-jk\left(r_1 + r_o - \frac{r_1 r_o}{r_1 + r_o}\right)}}{\sqrt{r_1 + r_o}}$$

$$\times \left[V_B\left(\frac{r_1 r_o}{r_1 + r_o}\ ,\ \theta_1 + \alpha\right) + V_B\left(\frac{r_1 r_o}{r_1 + r_o}\ ,\ 2\pi + \theta_1 - \alpha\right)\right] .$$

The singly diffracted field from edge ② $[H_2^{(1)}(2R,y)]$ is given by

$$(14)\qquad H_2^{(1)}(2R,y) = \frac{I e^{j\frac{\pi}{4}}}{\sqrt{2\pi}} \times \frac{e^{-jk\left(r_2 + r_o - \frac{r_2 r_o}{r_2 + r_o}\right)}}{\sqrt{r_2 + r_o}}$$

$$\times \left[V_B\left(\frac{r_2 r_o}{r_2 + r_o}\ ,\ \alpha - \theta_2\right) + V_B\left(\frac{r_2 r_o}{r_2 + r_o}\ ,\ 2\pi - \theta_2 - \alpha\right)\right] .$$

The singly diffracted wave from each wedge illuminates the opposite wedge. This wave in turn diffracts from the second wedge and contributes to the total field at the observation point $(2R, y)$. The doubly diffracted field from edge (1) $[H_1^{(2)}(2R, y)]$ is determined from the geometry of Fig. 6 and is evaluated as follows:

$$(15) \qquad D_{1G}^{(1)} = D_{2G}^{(1)} = \frac{I e^{j\frac{\pi}{4}}}{\sqrt{2\pi}} \times \sqrt{a}\; e^{jka} \times \frac{e^{-jk\left(a + r_o - \frac{r_o a}{r_o + a}\right)}}{\sqrt{a + r_o}}$$

$$\times \left[V_B\left(\frac{a\, r_o}{a + r_o}\,,\ \alpha - \frac{\pi}{2}\right) + V_B\left(\frac{a\, r_o}{a + r_o}\,,\ \frac{3\pi}{2} - \alpha\right)\right]$$

and

$$(16) \qquad U_1^{(2)} = \frac{e^{-jk\left(a + r_1 - \frac{a\, r_1}{a + r_1}\right)}}{\sqrt{a + r_1}}$$

$$\times \left[V_B\left(\frac{a\, r_1}{a + r_1}\,,\ \frac{\pi}{2} + \theta_1\right) + V_B\left(\frac{a\, r_1}{a + r_1}\,,\ \frac{3\pi}{2} + \theta_1\right)\right] \quad ,$$

then

$$(17) \qquad H_1^{(2)}(2R, y) = D_{2G}^{(1)} \times U_1^{(2)} \quad .$$

Similarly, the doubly diffracted component from edge 2 is given by

$$(18) \qquad U_2^{(2)} = \frac{e^{-jk\left(a + r_2 - \frac{a\, r_2}{a + r_2}\right)}}{\sqrt{a + r_2}}$$

$$\times \left[V_B\left(\frac{a\, r_2}{a + r_2}\,,\ \frac{\pi}{2} - \theta_2\right) + V_B\left(\frac{a\, r_2}{a + r_2}\,,\ \frac{3\pi}{2} - \theta_2\right)\right] \quad .$$

Then

$$(19) \qquad H_2^{(2)}(2R, y) = D_{1G}^{(1)} \times U_2^{(2)} \quad .$$

Equation (15) states $D_{1G}^{(1)} = D_{2G}^{(1)}$, which results from the general symmetry about the guide axis.

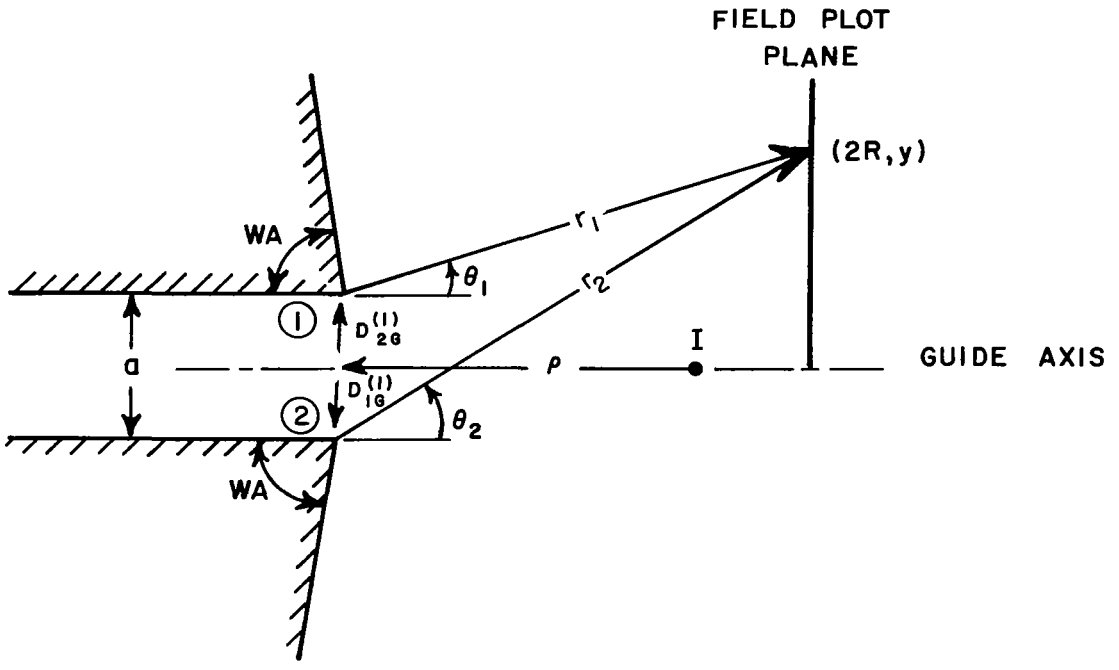

Fig. 6. Backscattering field plot geometry-the double diffraction component.

Finally, the value of the total field $[H_T(2R, y)]$ scattered from the actual waveguide at an arbitrary observation point $(2R, y)$ is the sum of each component as given by

$$H_T(2R, y) = H_{GO}(2R, y) + H_1^{(1)}(2R, y) + H_2^{(1)}(2R, y) + H_1^{(2)}(2R, y) + H_2^{(2)}(2R, y) \quad . \tag{20}$$

B. Representation of Solid Wedge Scattering by Cylindrical Wave Components

In order to apply wedge diffraction theory it is necessary to represent the scattered wave in terms of cylindrical wave components. In view of this the scattering from the waveguide wedges is represented in terms of scattering from the solid wedge and that resulting from the aperture (denoted as the aperture component). The aperture component

is the scattering from the complement of the solid wedge, as shown in Fig. 7, and is similar to the backscattering by a conducting strip of the same width. Thus the aperture component is well approximated as a cylindrical wave.

In this section the wave scattered by the solid wedge is determined for an arbitrary incident cylindrical wave and found to be adequately described by three cylindrical waves in the most general case. The field $[H_{TS}(2R, y)]$ at the observation point $(2R, y)$ as scattered by the solid wedge is given by the sum of the geometrical optics field $[H_{RS}(2R, y)]$ and the singly diffracted field $[H_{DS}(2R, y)]$. With the aid of Fig. 8 both these terms are computed as

$$(21) \qquad H_{DS}(2R, y) = \frac{e^{-jk\left(r_s + \rho' - \frac{r_s \rho'}{r_s + \rho'}\right)}}{\sqrt{r_s + \rho'}} \times \frac{I e^{j\frac{\pi}{4}}}{\sqrt{2\pi}}$$

$$\times \left[V_B\left(\frac{r_s \rho'}{r_s + \rho'}, -\theta_s\right) + V_B\left(\frac{r_s \rho'}{r_s + \rho'}, 2\pi - 2WA - \theta_s\right) \right]$$

and

$$(22) \qquad H_{RS}(2R, y) = \begin{cases} 0 & y \le y'_{min} \\ \dfrac{I e^{-jkr_i + j\frac{\pi}{4}}}{\sqrt{2\pi r_i}} & y > y'_{min} \end{cases},$$

where y'_{min} is the vertical distance in the field plot plane from the guide axis to the reflection shadow boundary. Thus the total field scattered by the solid wedge is given by

$$(23) \qquad H_{TS}(2R, y) = H_{RS}(2R, y) + H_{DS}(2R, y) .$$

The first cylindrical component determined from the scattered field by the solid wedge is the diffracted component. Before attempting to calculate this component it is necessary to present two general aspects of our theory. First, the diffracted field from a wedge is approximately cylindrical provided the observation point is sufficiently removed from the shadow boundaries (20° on either side). Second, the field of interest

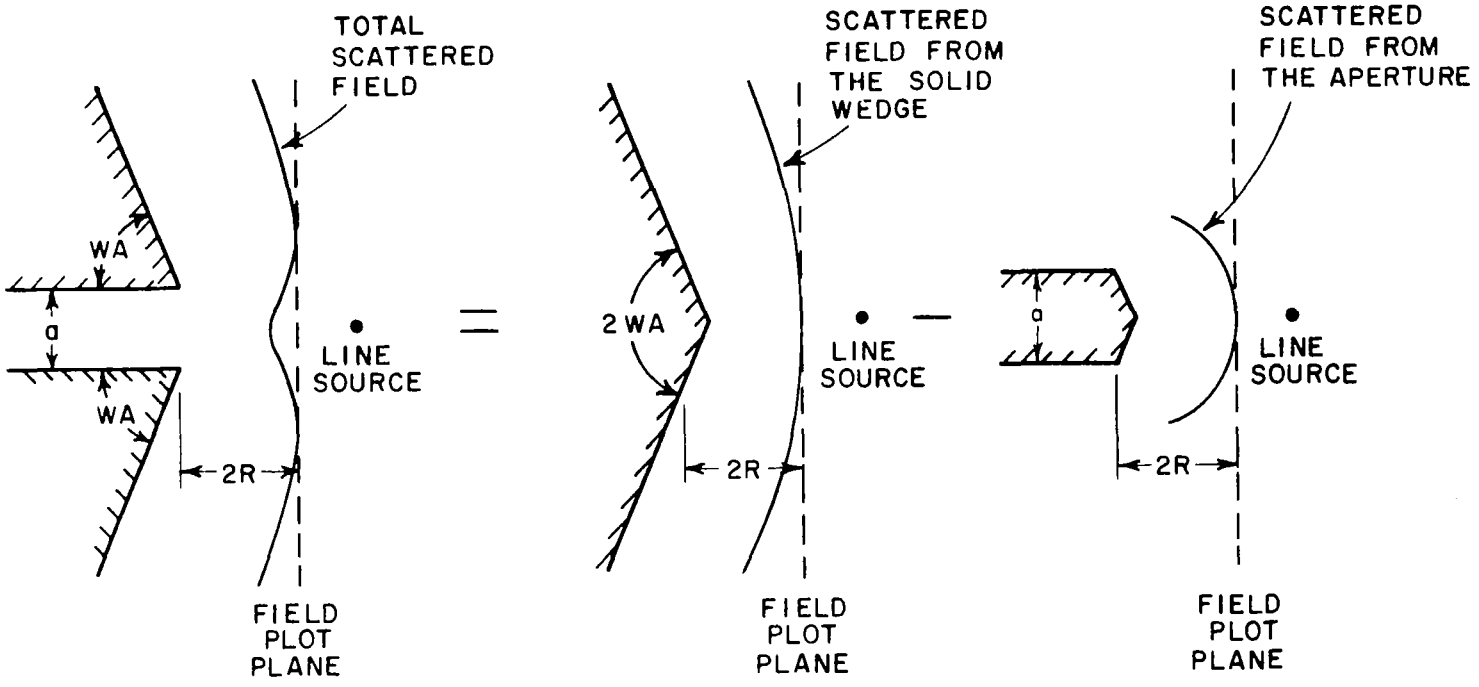

Fig. 7. The scattered field from the waveguide represented through the superposition of cylindrical wave components.

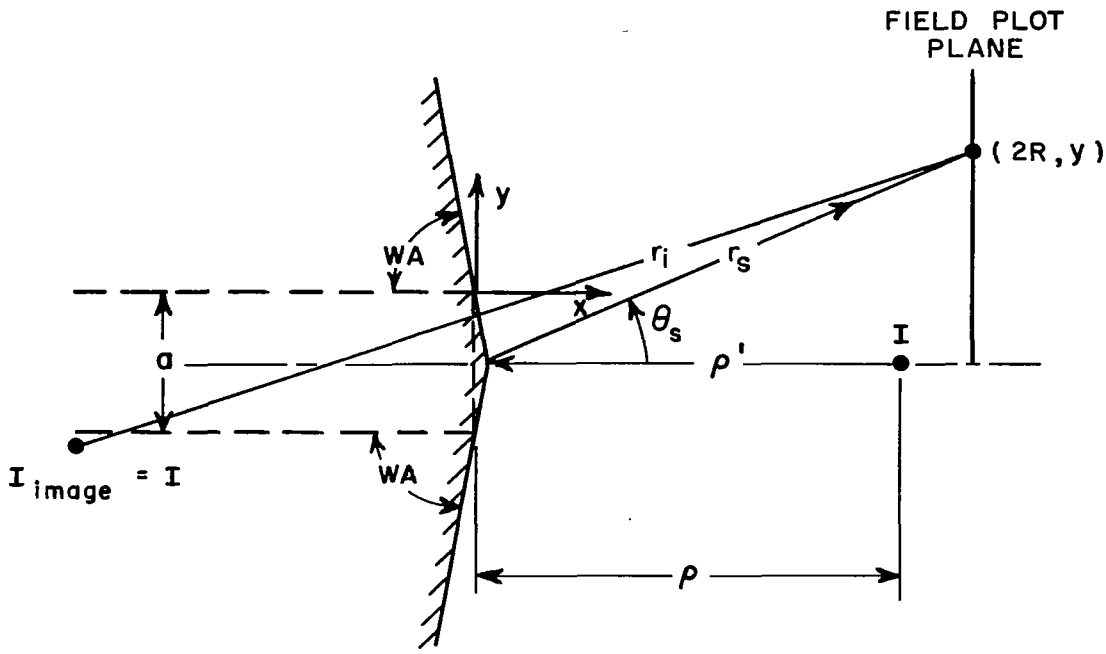

Fig. 8. Backscattering by the solid wedge.

is only that in the near zone of the projected guide aperture. Because of these aspects the problem divides into two cases.

> Case I: If the projected upper edge of the guide (y = 0) is less than 20° below the shadow boundary, then the diffracted term is determined from the diffracted field value at the point 20° above the shadow boundary ($y = y_a$), as shown in Fig. 9a.
>
> Case II: If the projected upper edge of the guide (y = 0) is at least 20° below the shadow boundary, then the diffracted term is determined by the diffracted field value on the guide axis (y = -a/2) in the field plot plane, as shown in Fig. 9b.

These two cases result in necessarily different calculations and are studied separately as follows:

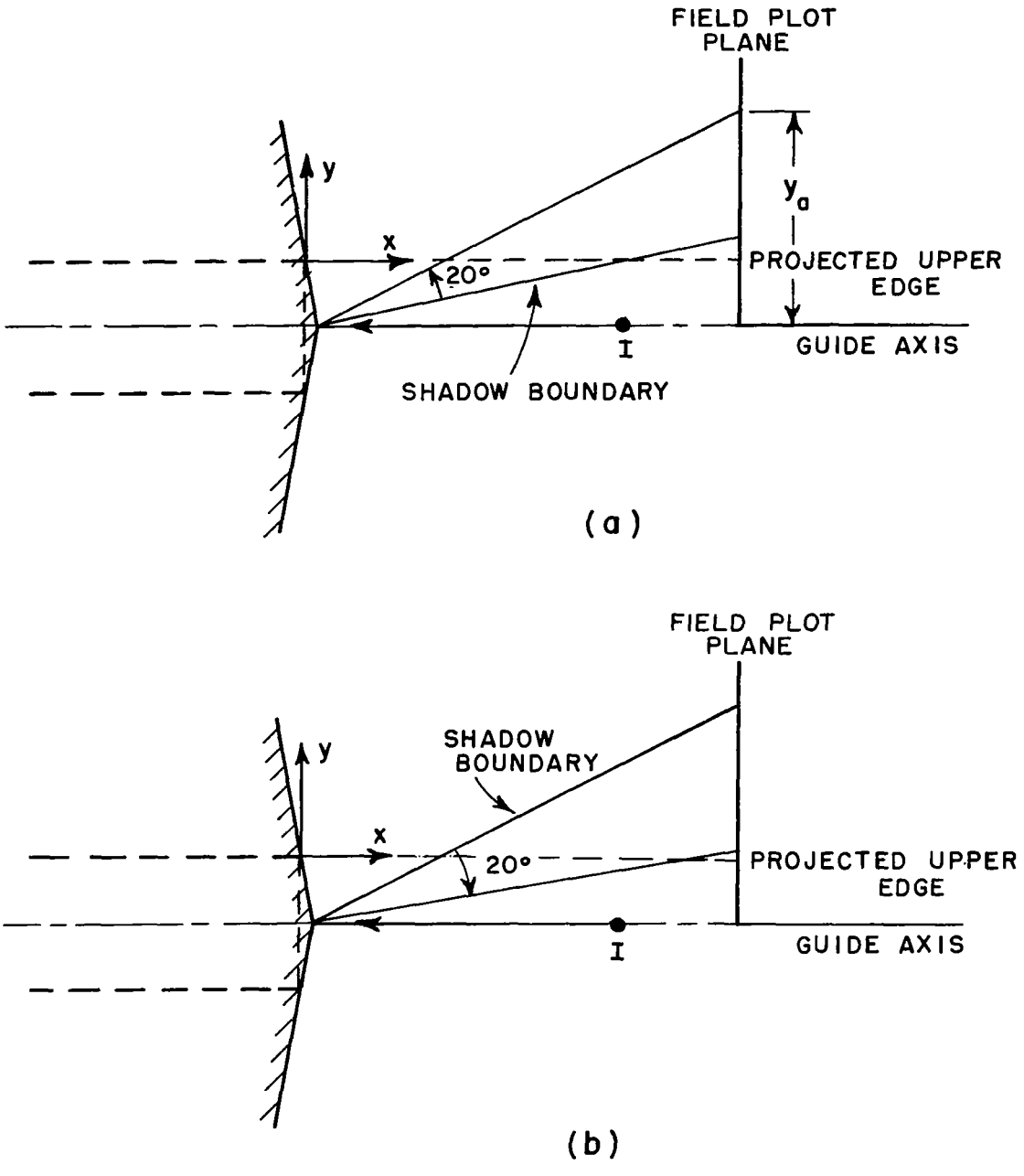

Fig. 9. (a) Case I of the solid wedge scattering.
(b) Case II of the solid wedge scattering.

Case I

The diffracted component is a cylindrical wave radiated by a **line** source, whose current (I_D) is determined from the diffracted field value at the observation point ($2R, y_a$). The position of this equivalent line source is at the apex of the solid wedge. It follows that

$$(24) \qquad I_D = H_{DS}(2R, y_a)\sqrt{2\pi r_s}\; e^{jkr_s - j\frac{\pi}{4}} \quad ,$$

where r_s is the distance from the apex to the observation point ($2R, y_a$). Then the diffracted component which approximates the actual diffracted field is given by

$$(25) \qquad H_{DA}(2R, y) = \frac{I_D\, e^{-jkr_D + j\frac{\pi}{4}}}{\sqrt{2\pi r_D}} \quad ,$$

where r_D is defined in Fig. 10.

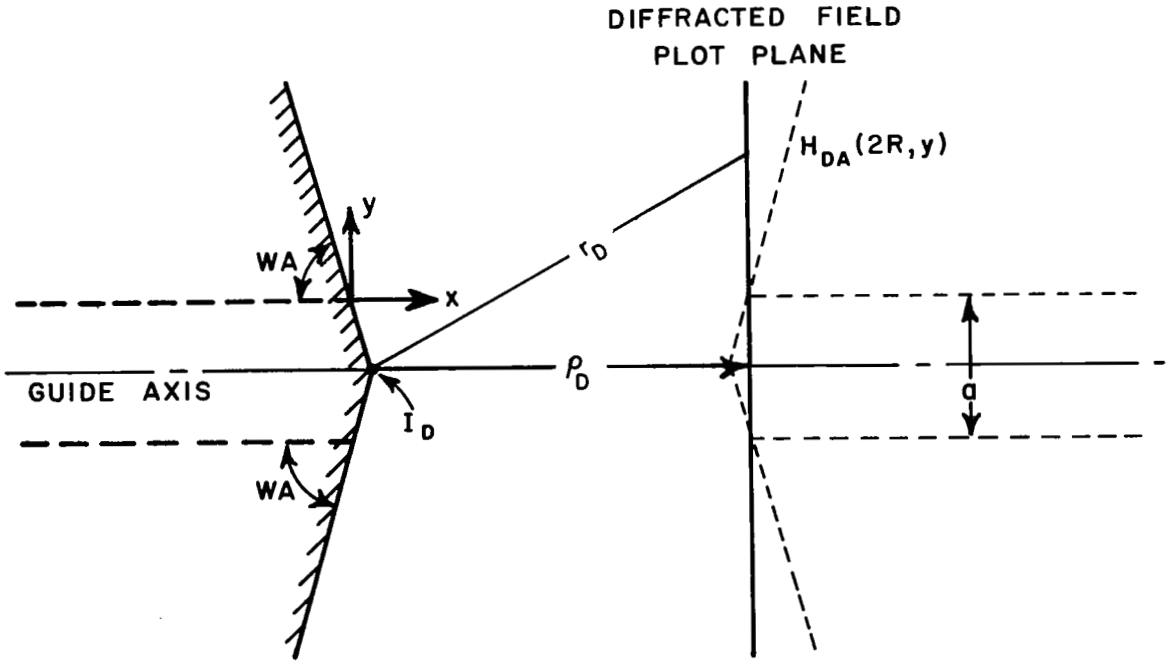

Fig. 10. The equivalent line source representing the solid wedge diffracted field (Case I).

The geometrical optics field reflected from the solid wedge is not directly applicable to this analysis because its radiated field is discontinuous. Consequently, a uniform cylindrical wave which approximates the geometrical optics field is determined. The source for this geometrical component is a line source located on the guide axis at a position (ρ_R) from the x = 2R plane as shown in Fig. 11. The position

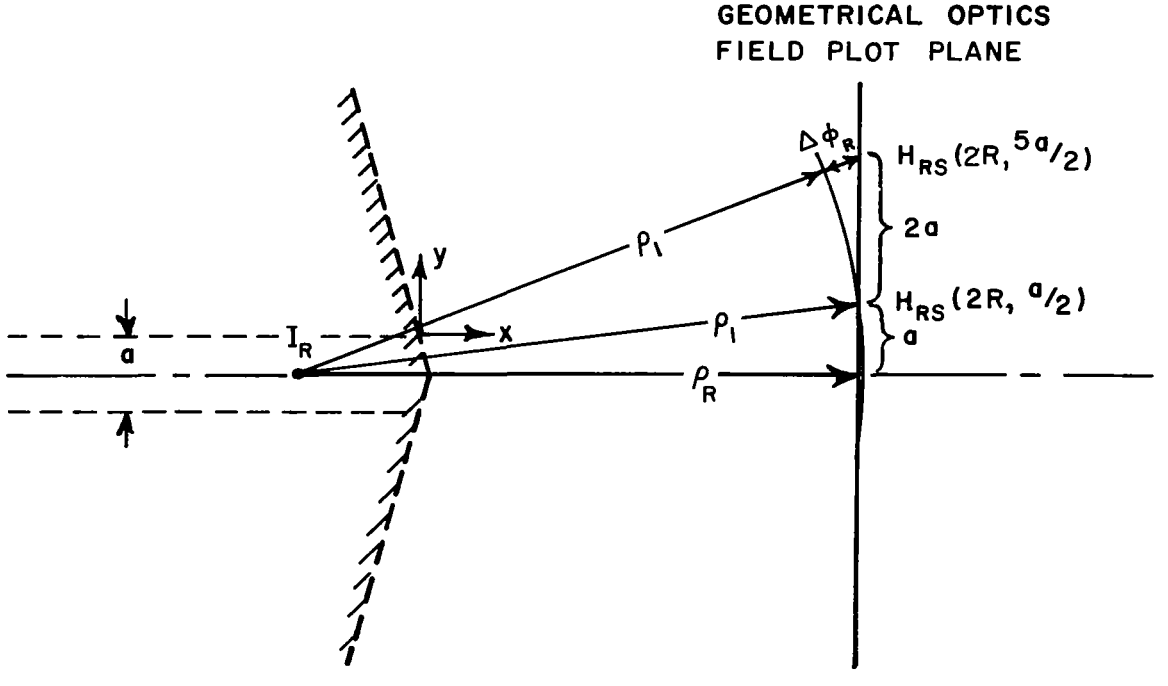

Fig. 11. The equivalent line source representing the solid wedge reflected field.

(ρ_R) is determined by the phase difference ($\Delta\phi_R$) in the actual reflected field [$H_{RS}(2R, y)$] at the observation points (2R, a/2) and (2R, 5a/2). By geometry

$$\rho_R = \sqrt{\frac{16a^4}{\Delta\phi_R^2} - 5a^2 + \frac{\Delta\phi^2}{4}} \quad , \tag{26}$$

where $\Delta\phi_R$ = phase difference in wavelengths. The current (I_R) for the geometrical component is calculated from the true geometrical optics field [$H_{RS}(2R, y)$] at the observation point (2R, a/2) and is given as

$$(27) \qquad I_R = \sqrt{2\pi\rho_1}\; e^{jk\rho_1 - j\frac{\pi}{4}}\; H_{RS}(2R, a/2) \quad ,$$

where ρ_1 is the distance from the line source to the observation point $(2R, a/2)$. Then the geometrical component which approximates the geometrical optics field is given by

$$(28) \qquad H_{RA}(2R, y) = \frac{I_R\, e^{-jkr_R + j\frac{\pi}{4}}}{\sqrt{2\pi r_R}} \quad ,$$

where r_R is the distance from the line source to the observation point $(2R, y)$.

By subtracting the approximate geometrical optics and diffracted fields from the true solid wedge scattered field, there is found to be a residual error in the approximation, which is of particular interest in the region from the shadow boundary to the guide axis. This deviation, which has the form of a cusp, is attributed to the discontinuities in the reflected and diffracted fields across the shadow boundary. These discontinuities are such that their sum gives a continuous total field but not a field that can be adequately represented by two uniform cylindrical waves. However, it is found that this deviation field is not great and for all practical purposes can be represented as a uniform cylindrical wave. This cusp component, which approximates the deviation field, has a line source positioned along the guide axis at a distance ρ_C from the $x = 2R$ plane as shown in Fig. 12. The magnitude of ρ_C is determined by the phase difference $(\Delta\phi_s)$ in the deviation field $[H_{TS}(2R, y) - (H_{DA}(2R, y) + H_{RA}(2R, y))]$ at the observation points $(2R, -a/2)$ and $(2R, a/2)$. Hence,

$$(29) \qquad \rho_C = \frac{a^2}{2\Delta\phi_s} - \frac{\Delta\phi_s}{2} \quad .$$

The current (I_C) for the cusp component is computed from the deviation field at the observation point $(2R, -a/2)$ and is given by

$$(30) \qquad I_C = \sqrt{2\pi\rho_C}\; e^{jk\rho_C - j\frac{\pi}{4}}$$

$$\times[H_{RA}(2R, -a/2) + H_{DA}(2R, -a/2) - H_{TS}(2R, -a/2)] \quad .$$

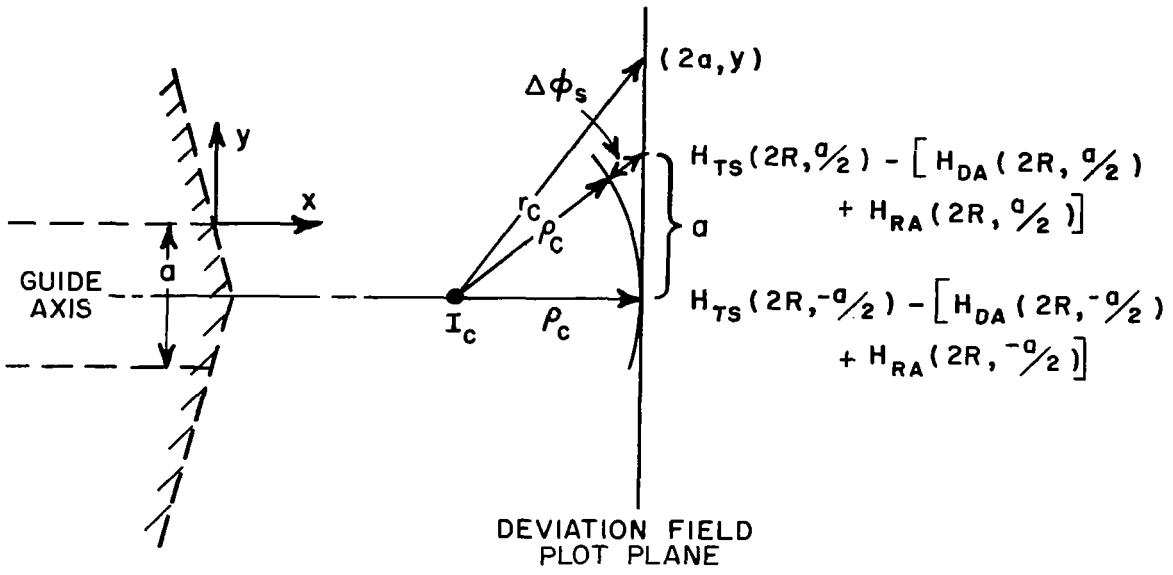

Fig. 12. Deviation field, or cusp, equivalent line source.

Thus, the resulting cusp field $[H_{CA}(2R, y)]$ that approximates the deviation field is given by

$$H_{CA}(2R, y) = \frac{I_C \, e^{-jkr_C + j\frac{\pi}{4}}}{\sqrt{2\pi r_C}} \quad , \tag{31}$$

where r_C is the distance from the cusp line source position to the observation point $(2R, y)$ as shown in Fig. 12.

Finally, the approximate total solid field $[H_{ATS}(2R, y)]$ is the sum of the three components as given by

$$H_{ATS}(2R, y) = H_{DA}(2R, y) + H_{RA}(2R, y) - H_{CA}(2R, y). \tag{32}$$

Calculations have shown that this resulting approximate field describes the true solid-wedge scattered field very adequately in the near zone of the projected guide aperture.

Case II

If the projected upper edge of the guide aperture is at least 20° below the shadow boundary, then the approximate total solid field $[H_{ATS}(2R, y)]$ is adequately described by a single cylindrical wave because of the cylindrical nature of the diffracted field across the projected guide aperture. Again, the diffracted field is generated by a line source located at the apex of the solid wedge. However, the current (I_D) is determined by the true solid-field value at the observation point ($2R, -a/2$) and is given as

$$(33) \qquad I_D = \sqrt{2\pi\rho_D}\; e^{jk\rho_D - j\frac{\pi}{4}} \left[H_{TS}(2R, -a/2)\right] \quad ,$$

where ρ_D is the distance along the guide axis from the apex to the $x = 2R$ plane, as shown in Fig. 13. With this line source known, the approximate total solid field is computed as

$$(34) \qquad H_{ATS}(2R, y) = \frac{I_D\, e^{-jkr_\ell + j\frac{\pi}{4}}}{\sqrt{2\pi r_\ell}} \quad ,$$

where r_ℓ is the distance from the edge to an arbitrary observation point ($2R, y$).

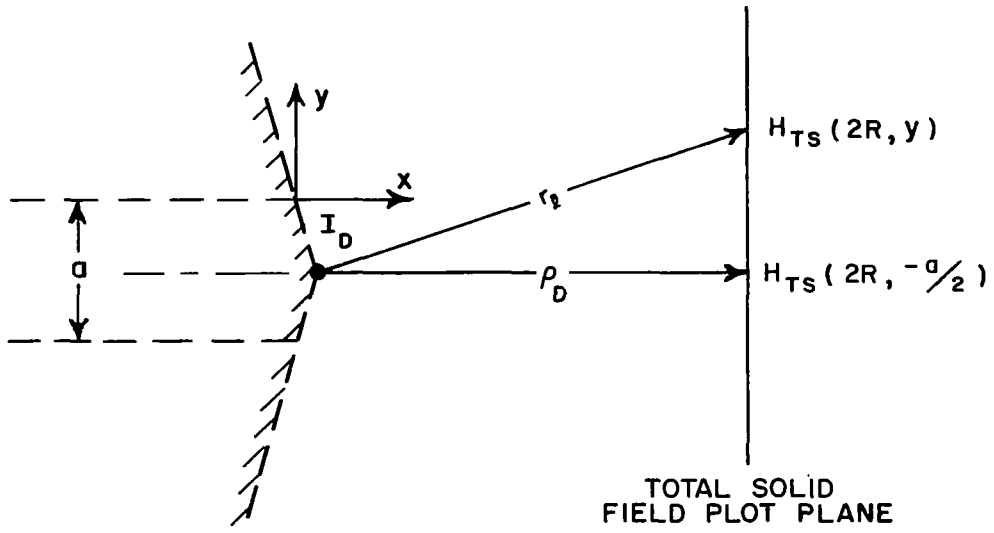

Fig. 13. The equivalent line source representing the solid wedge diffracted field (Case II).

C. Aperture Component of the Scattered Field

The difference between the approximate total solid field $[H_{ATS}(2R, y)]$ and the true waveguide field $[H_T(2R, y)]$ is attributed to the presence of the waveguide aperture and is basically a cylindrical wave from the center of the aperture. Consequently, the aperture component is approximated as that radiated from a line source. The position (ρ_A) of this aperture component line source is calculated from the phase deviation $(\Delta\phi_A)$ between the difference field $[H_T(2R, y) - H_{ATS}(2R, y)]$ at the observation points $(2R, -a/2)$ and $(2R, 0)$. With the aid of Fig. 14,

$$\rho_A = \frac{(a/2)^2}{2\Delta\phi_A} - \frac{\Delta\phi_A}{2} \qquad (35)$$

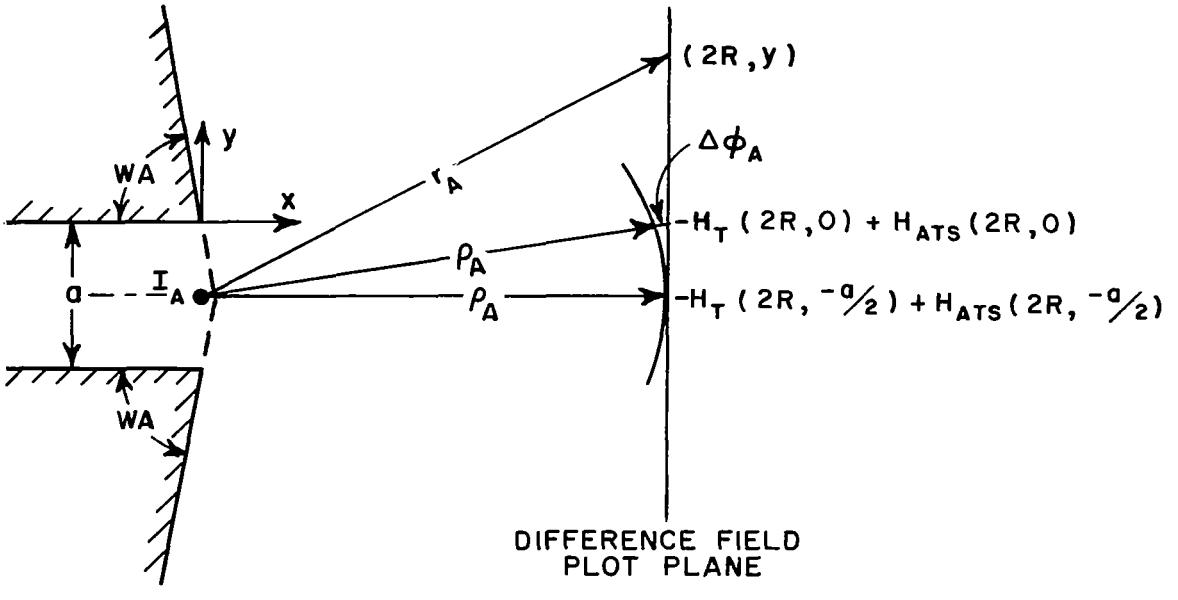

Fig. 14. Equivalent line source representation of the aperture component.

The current (I_A) associated with this source is specified by the difference field $[-H_T(2R, y) + H_{ATS}(2R, y)]$ at the observation point $(2R, -a/2)$ and is given by

$$I_A = \sqrt{2\pi\rho_A}\; e^{jk\rho_A - j\frac{\pi}{4}} [-H_T(2R, -a/2) + H_{ATS}(2R, -a/2)] \; . \qquad (36)$$

Then the aperture component $[H_A(2R, y)]$ is computed by the general line-source field formula as

$$H_A(2R, y) = \frac{I_A e^{-jkr_A + j\frac{\pi}{4}}}{\sqrt{2\pi r_A}} , \qquad (37)$$

where r_A is the distance from the source to the observation point $(2R, y)$.

The total field $[H_{TA}(2R, y)]$ scattered by the waveguide wedges is approximated as the superposition of the approximate scattering from the solid wedge and the aperture component such that in the most general case it consists of four cylindrical wave components and is given by

$$H_{TA}(2R, y) = H_{ATS}(2R, y) - H_A(2R, y). \qquad (38)$$

Whether the approximate field scattered by the solid wedge is described by three line-source waves (Case I) or by one line-source wave (Case II), the total field scattered by the waveguide wedges is accurately approximated. This makes it possible to use our basic theory (wedge diffraction) in the transient or successive bounce approach, as will be discussed in the next section.

III. REFLECTION COEFFICIENT ANALYSIS

As discussed in Section I, the first-bounce wave of the waveguide may be approximated by an equivalent cylindrical wave. The reflection coefficient contribution of the first-bounce wave is then given by Eq. (7).

Using the mechanism of cylindrical wave scattering as derived in Section II, the first-bounce cylindrical wave, when scattered by the guide aperture, produces a second-bounce wave composed of four (Case I) or two (Case II) component cylindrical waves. As shown in Fig. 15 the second-bounce wave is seen to be that from the superposition of four (Case I) or two (Case II) equivalent line sources.

The reflection coefficient contributions from the second-bounce wave is computed in the same manner as $\Gamma^{(1)}$, the first-bounce contribution. Using the line source to waveguide coupling expression of Eq. (3) and the approximate line sources (currents and locations)

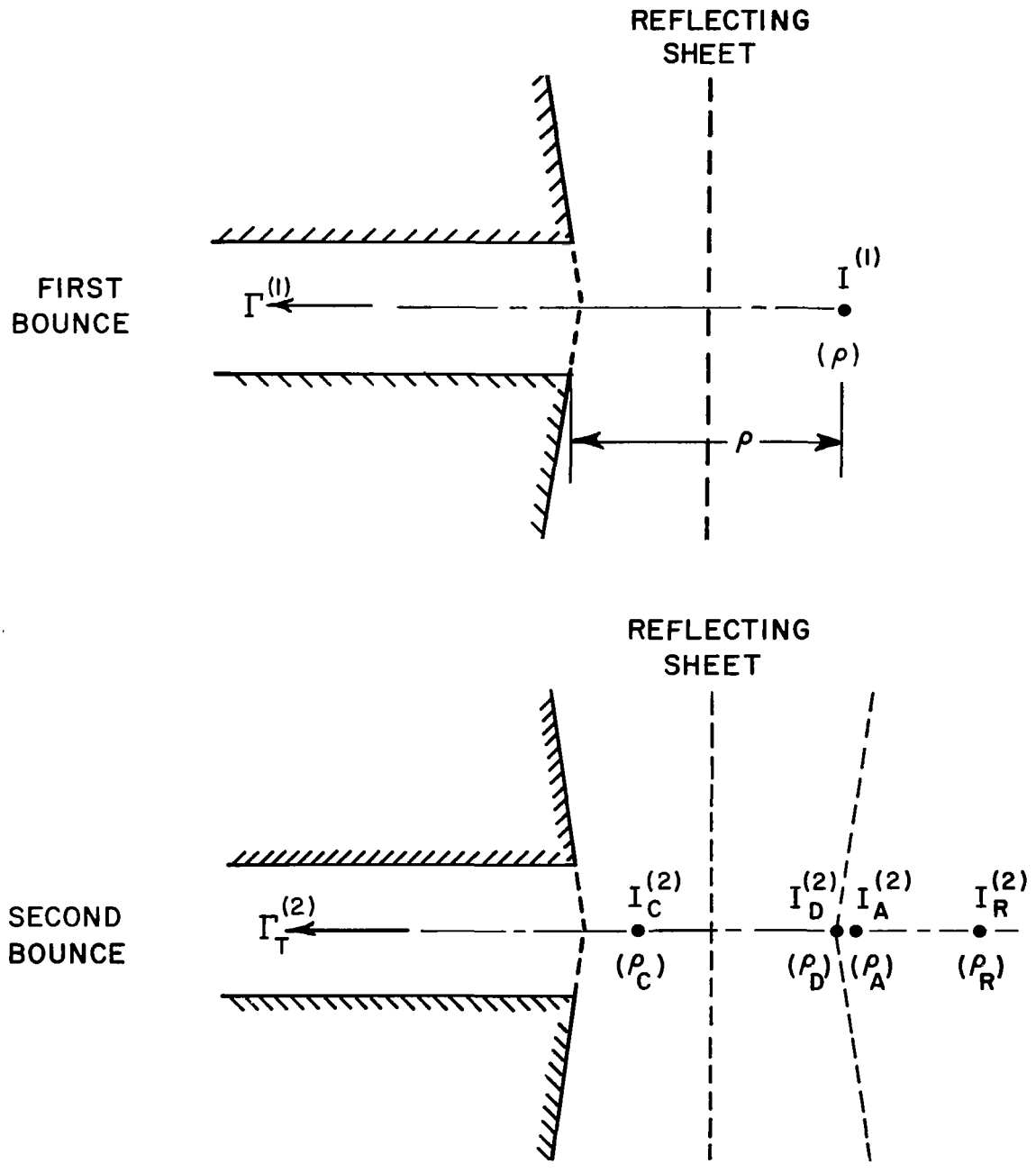

Fig. 15. The generation of the second-bounce equivalent line sources.

as determined by the method of Section II, the second-bounce reflection coefficient contributions are given by

$$\Gamma^{(2)}(1) = \frac{I_C^{(2)}}{a}\sqrt{\frac{\lambda}{2\pi}}\, H_T(\rho_C^{(2)}) \quad , \tag{39}$$

$$\Gamma^{(2)}(2) = \frac{I_D^{(2)}}{a}\sqrt{\frac{\lambda}{2\pi}}\, H_T(\rho_D^{(2)}) \quad , \tag{40}$$

$$\Gamma^{(2)}(3) = \frac{I_A^{(2)}}{a}\sqrt{\frac{\lambda}{2\pi}}\, H_T(\rho_A^{(2)}) \quad , \tag{41}$$

and

$$\Gamma^{(2)}(4) = \frac{I_R^{(2)}}{a}\sqrt{\frac{\lambda}{2\pi}}\, H_T(\rho_R^{(2)}) \quad , \tag{42}$$

where H_T is computed by the method in Reference 1, Section IIA. The total second-bounce contribution to the reflection coefficient is then given by

$$\Gamma_T^{(2)} = \sum_{n=1}^{4} \Gamma^{(2)}(n) \quad . \tag{43}$$

It should be noted that only the situation for Case I, where there are four resultant line sources, is shown in Fig. 15. For Case II, only I_A and I_D will be present. The computer program used in the computation is designed to automatically decide from the geometries whether Case I or II should apply. Subsequent discussions will treat only the more complicated Case I.

In a manner similar to the generation of the second-bounce wave with its four cylindrical components by the first-bounce wave, each of the four cylindrical components of the second-bounce wave will in turn be scattered by the guide and form four subsequent cylindrical waves. These then reflect from the reflecting sheet to form the third-bounce wave. Thus the third-bounce wave will have a maximum of sixteen line sources, as can be seen in Fig. 16. The reflection coefficient contributions from the third bounce are then computed in exactly the same manner as that from the second bounce.

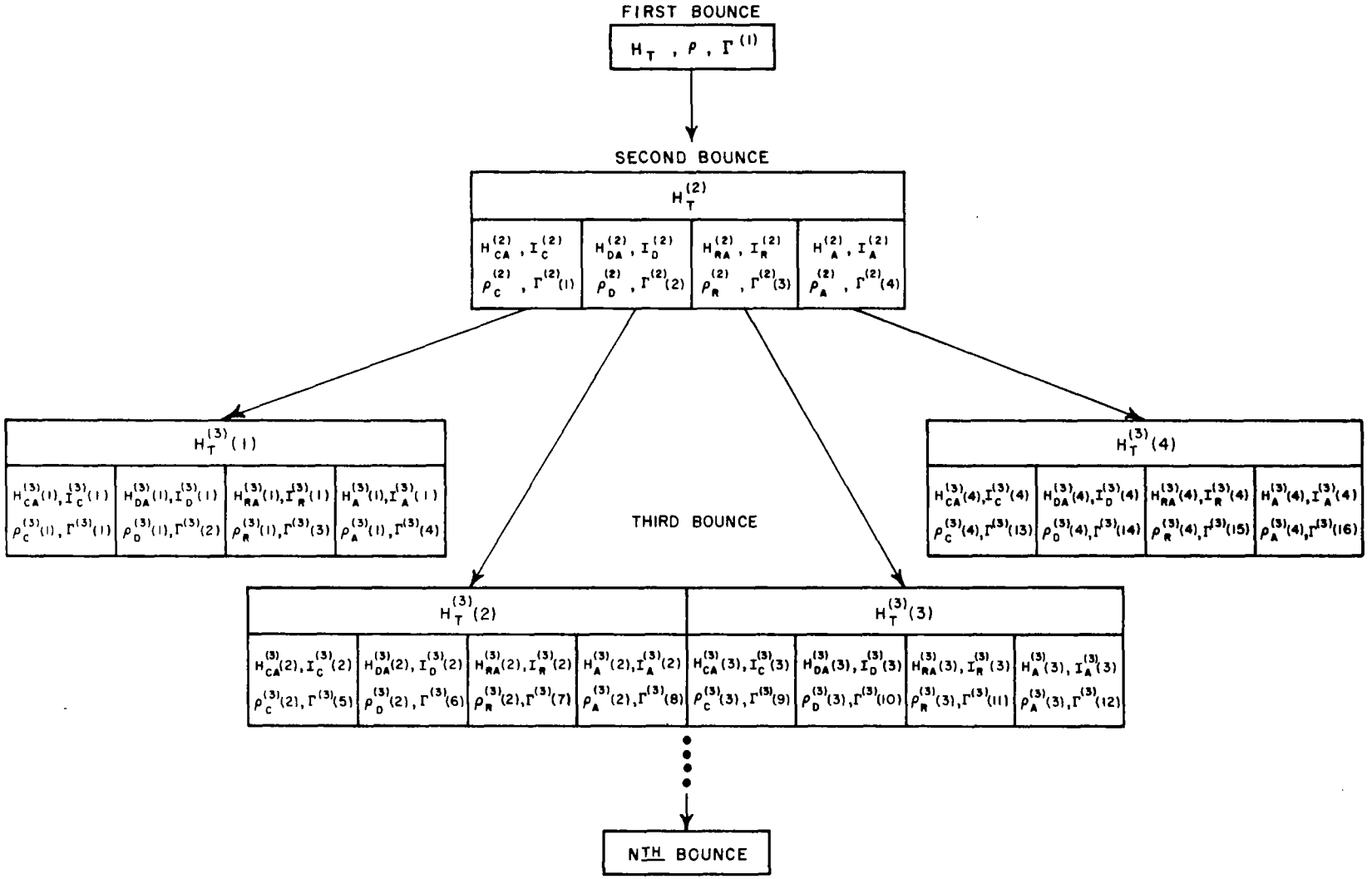

Fig. 16. The iterative process of the formation of multiple bounces.

The iterative process of Fig. 16 is continued to calculate the higher-order bounces. The total reflection coefficient is then given by the summation of all bounce contributions as

$$\Gamma_T = \Gamma_S + \sum_{n=1}^{\infty} \sum_{m=1}^{4n} \Gamma^{(n)}(m) \quad , \tag{44}$$

where the superscript (n) denotes the bounce order.

IV. RESULTS

Calculations of the total reflection coefficient of the large wedge angle guide illuminating a perfectly reflecting sheet were made with the aid of a Scatran program on the IBM 7094 digital computer. Values were computed for various guide geometries and for reflector spacings ranging from 0.6λ to 1.5λ. Depending on wedge angle, either three or four bounces were used in the computations.

In order to economize computation time, the following approximation is used. From sample calculations at selected reflector spacings, it was found that the contribution of each bounce wave to the reflection coefficient, when plotted versus the reflector spacing, exhibits a magnitude variation very close to an exponential decay and a nearly linear phase variation. By calculating the reflection coefficient at widely spaced reflecting sheet locations, the exponential decays for the magnitudes of the various bounce components and their corresponding linear phase variations were determined by curve fitting approximations. The phasor sum of these bounce component curves with the self-reflection coefficient then yields the total reflection coefficient with a minimum expenditure of computer time.

Figures 17 through 26 show the results for a 0.278λ guide for various wedge angles. In Fig. 17 the magnitude of the bounce contributions to Γ_T is shown as a function of reflector spacing for wedge angles equal to 75°, 85°, and 90°. The results for the ground-plane mounted guide (WA = 90°) were computed in Reference 1, Chapter V. It can be seen that the higher-order bounce contributions become less significant as wedge angle decreases.

Figures 18 and 19 give the magnitude and phase of the total reflection coefficient for the 75° wedge angle case as computed by both the cylindrical wave approach of this report and the plane wave method of Reference 1, Chapter IV. Only the first three bounces were needed to obtain good convergence for the cylindrical wave approach. The measured results were obtained with a sectoral horn[1,5] simulating the parallel-plate waveguide.

Comparison between the reflection coefficient magnitude and phase as computed by both the plane-wave approach and the cylindrical-wave approach with three bounces is shown in Figs. 20 and 21 for the 80° wedge angle case. The 85° wedge angle case is shown in Figs. 22 and 23, with the results including both three and four bounces for the cylindrical wave approach. Figures 24 and 25 present the comparison for the 88° wedge angle case. Figure 26 gives the reflection coefficient magnitude as a function of wedge angle as computed by the cylindrical wave method. It is apparent from the above figures that as the wedge angle approaches 90°, more and more bounce contributions must be summed before convergent results can be obtained. However, because of inherent numerical inaccuracies in the computer program, only up to four bounces were considered, even though the analysis can yield many more.

The results for a 0.423λ wide guide are shown in Figs. 27 through 30. Figures 27 and 28 give the reflection coefficient magnitude and phase for the 75° wedge angle case computed by both the plane-wave method and the cylindrical-wave method with three bounces. Four bounces were included in the results for the 85° wedge angle case in Figs. 29 and 30.

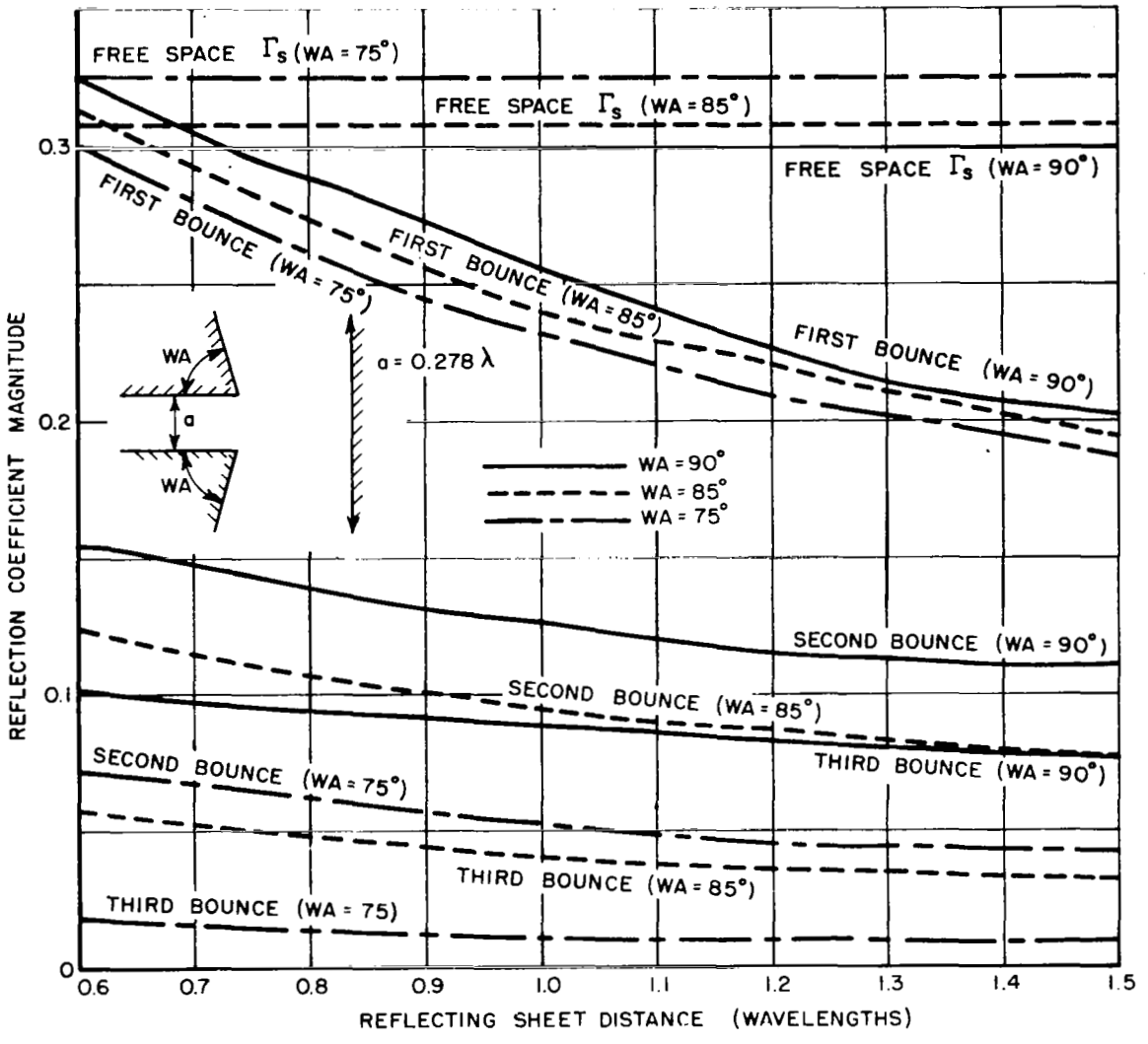

Fig. 17. Bounce contributions for WA = 75°, 85°, 90° calculated by the cylindrical wave approach.

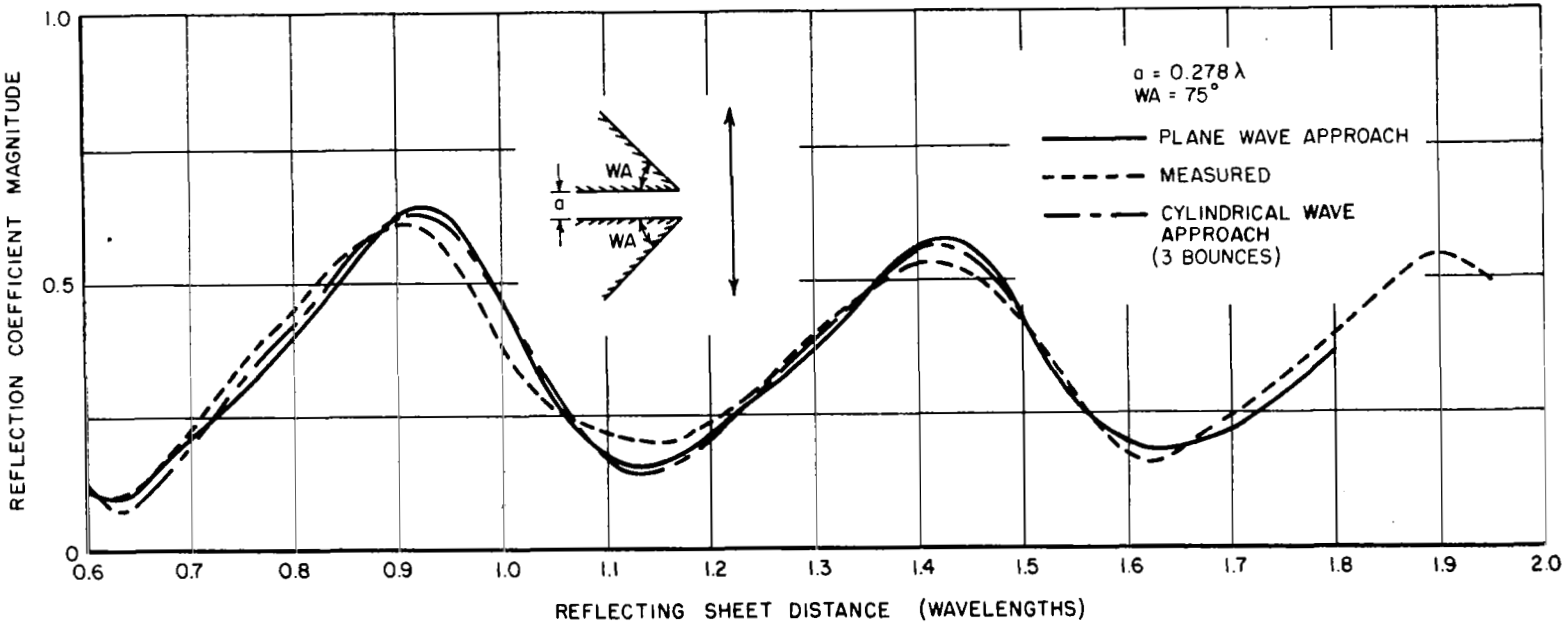

Fig. 18. Comparison of measured reflection coefficient magnitude with those calculated by both the plane wave and cylindrical wave approach (a = 0. 278λ, WA = 75°).

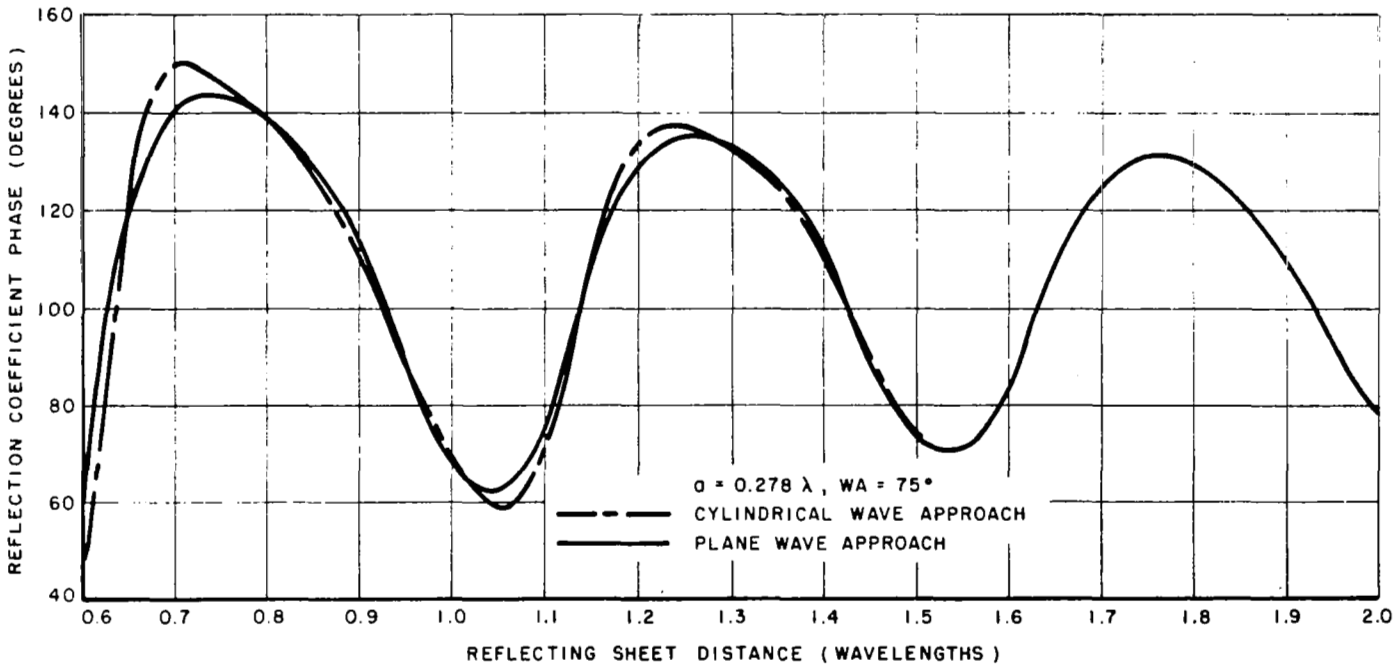

Fig. 19. Reflection coefficient phase comparison (a = 0. 278λ, WA = 75°).

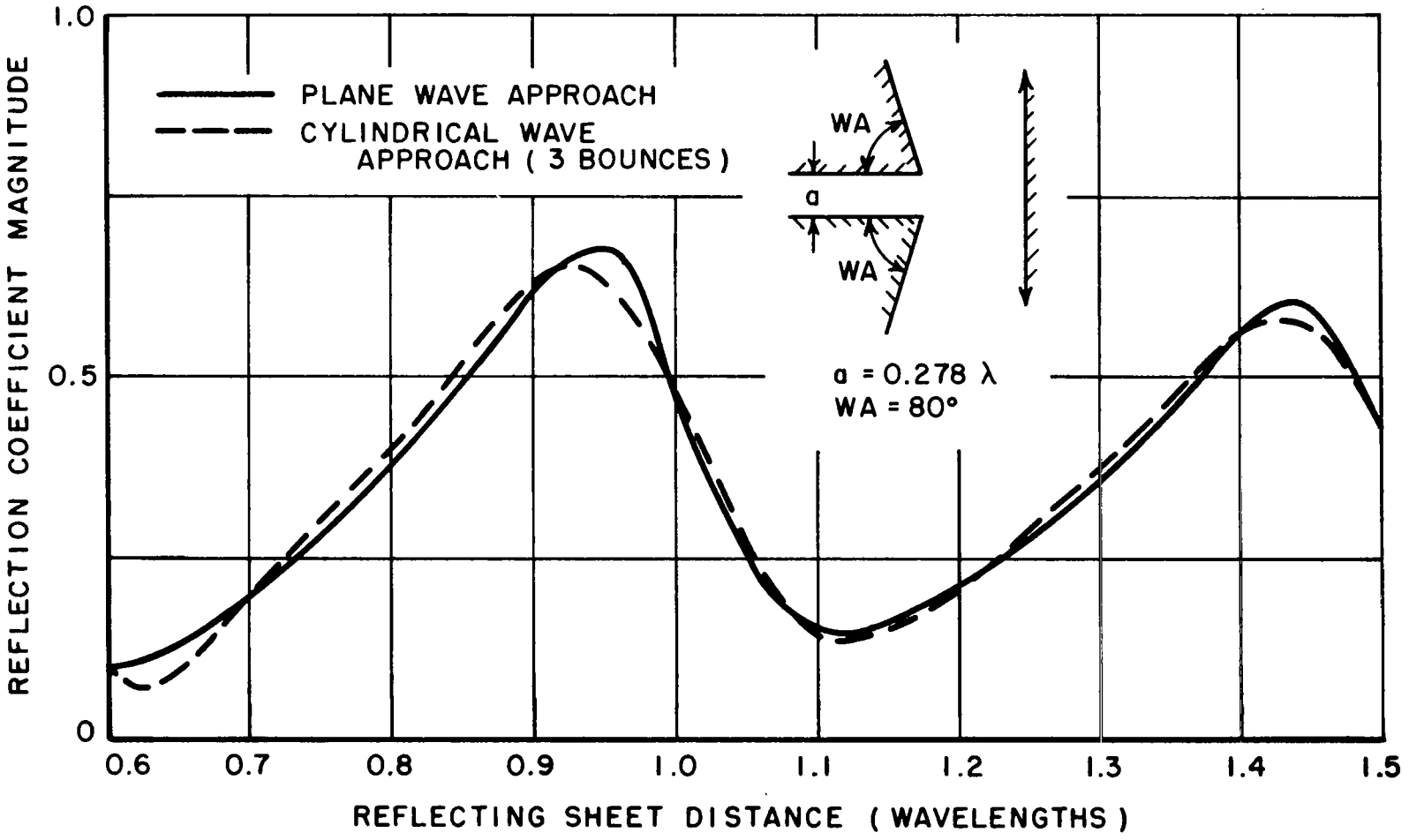

Fig. 20. Comparison of the reflection coefficient magnitude calculated by the plane wave approach and the cylindrical wave approach (a = 0. 278λ, WA = 80°).

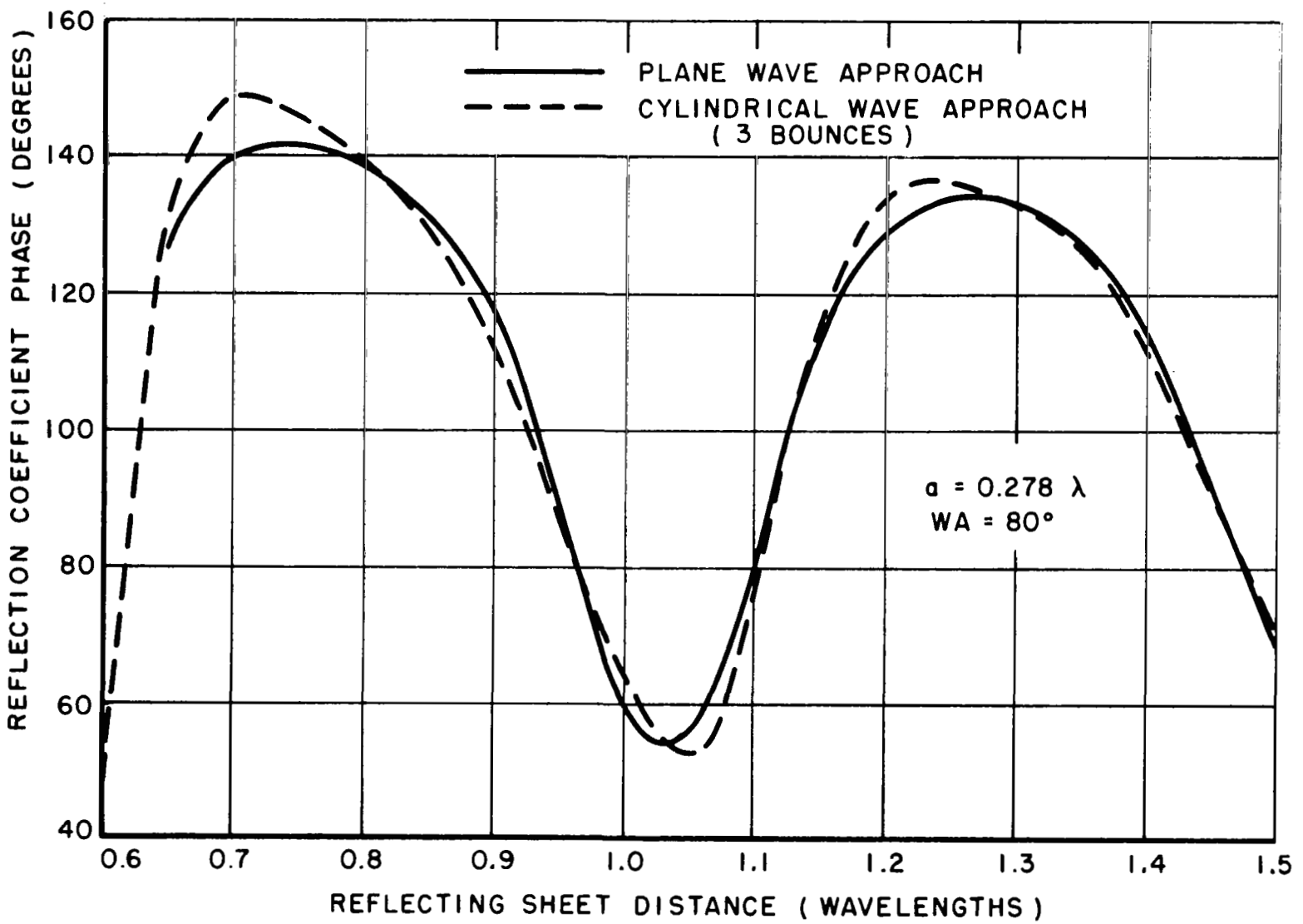

Fig. 21. Reflection coefficient phase comparison (a = 0.278λ, WA = 80°).

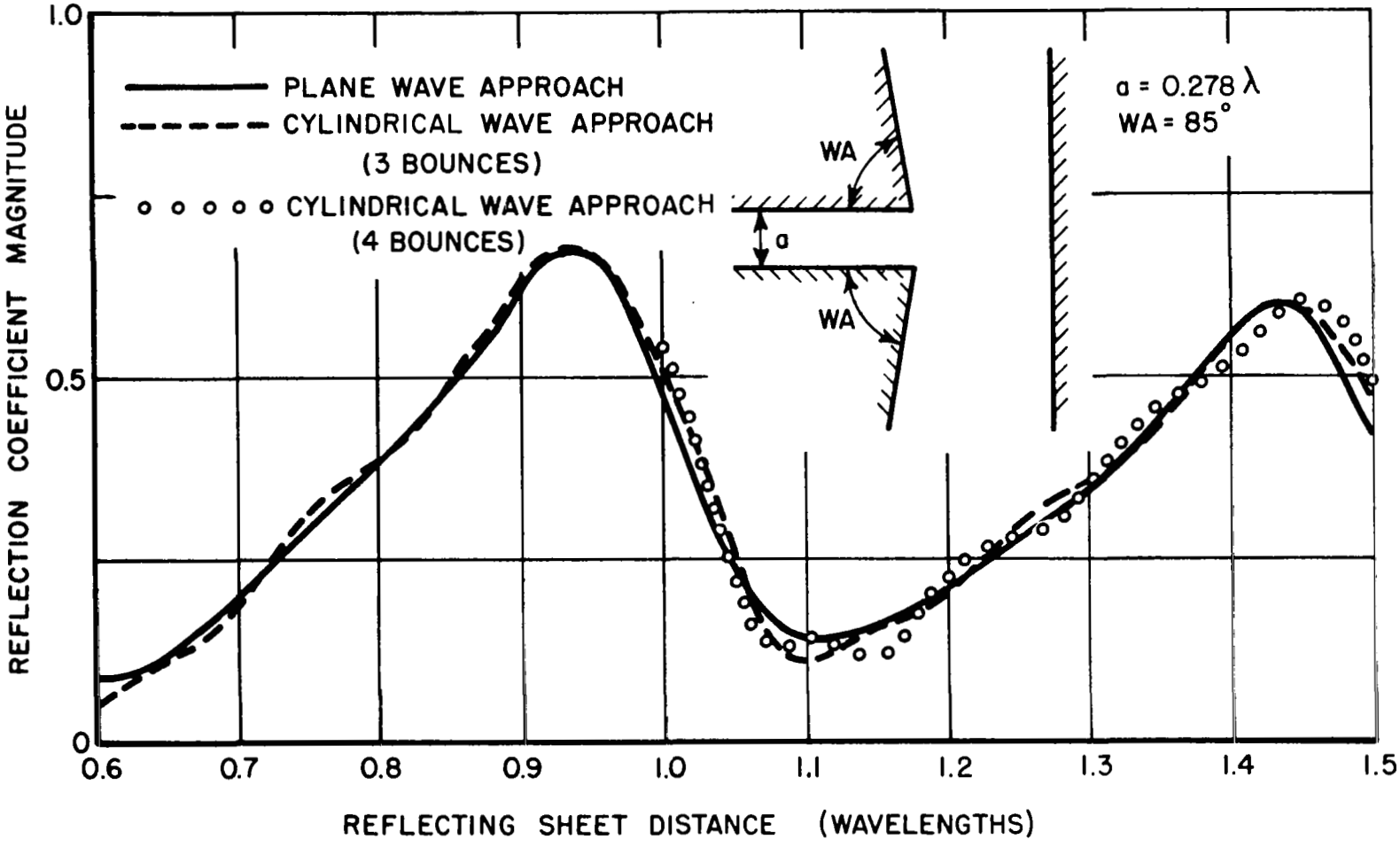

Fig. 22. Comparison of the reflection coefficient magnitude calculated by the plane wave approach and by the cylindrical wave approach with three and four bounces ($a = 0.278\lambda$, $WA = 85°$).

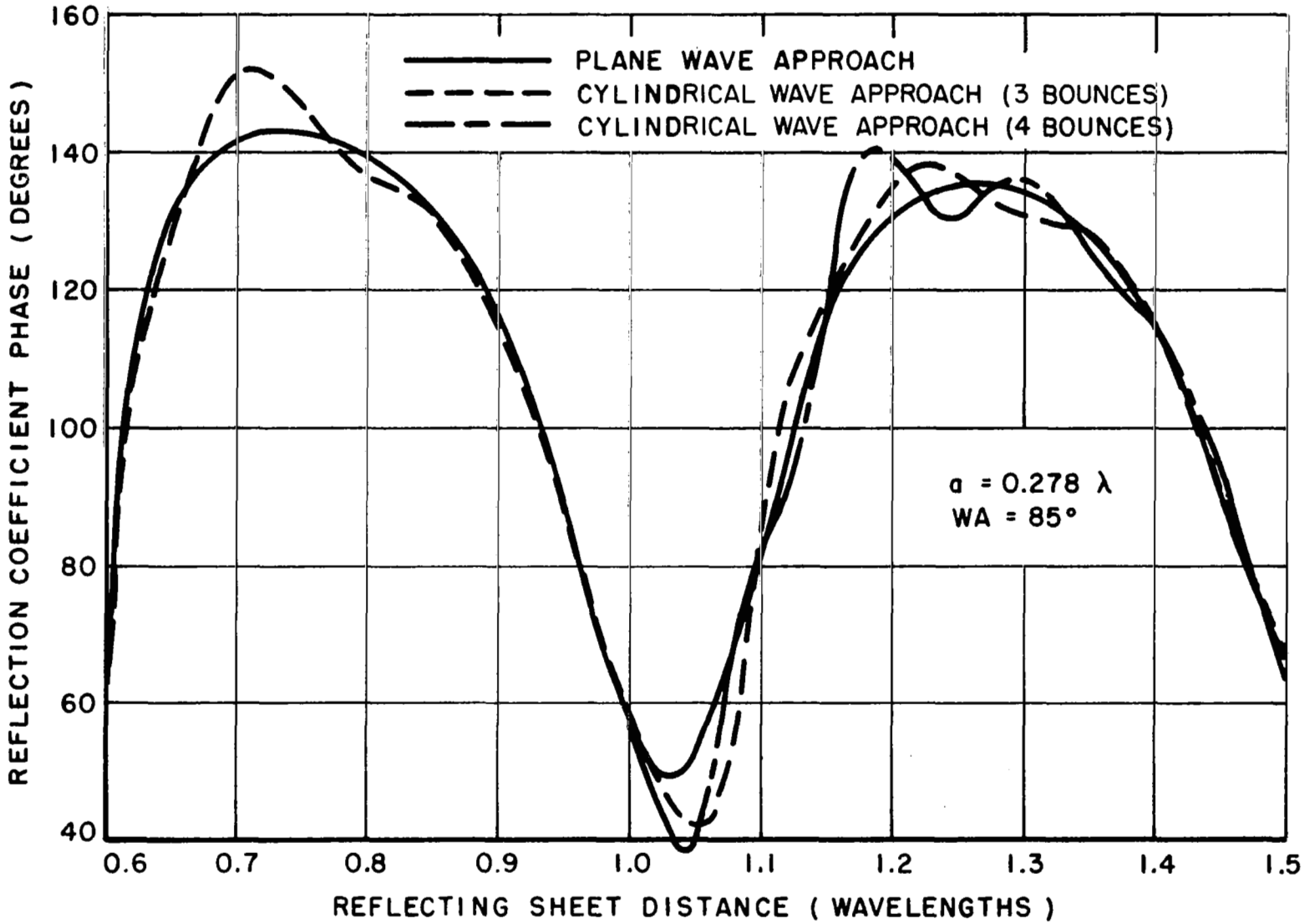

Fig. 23. Comparison of reflection coefficient phase (a = 0. 278λ, WA = 85°).

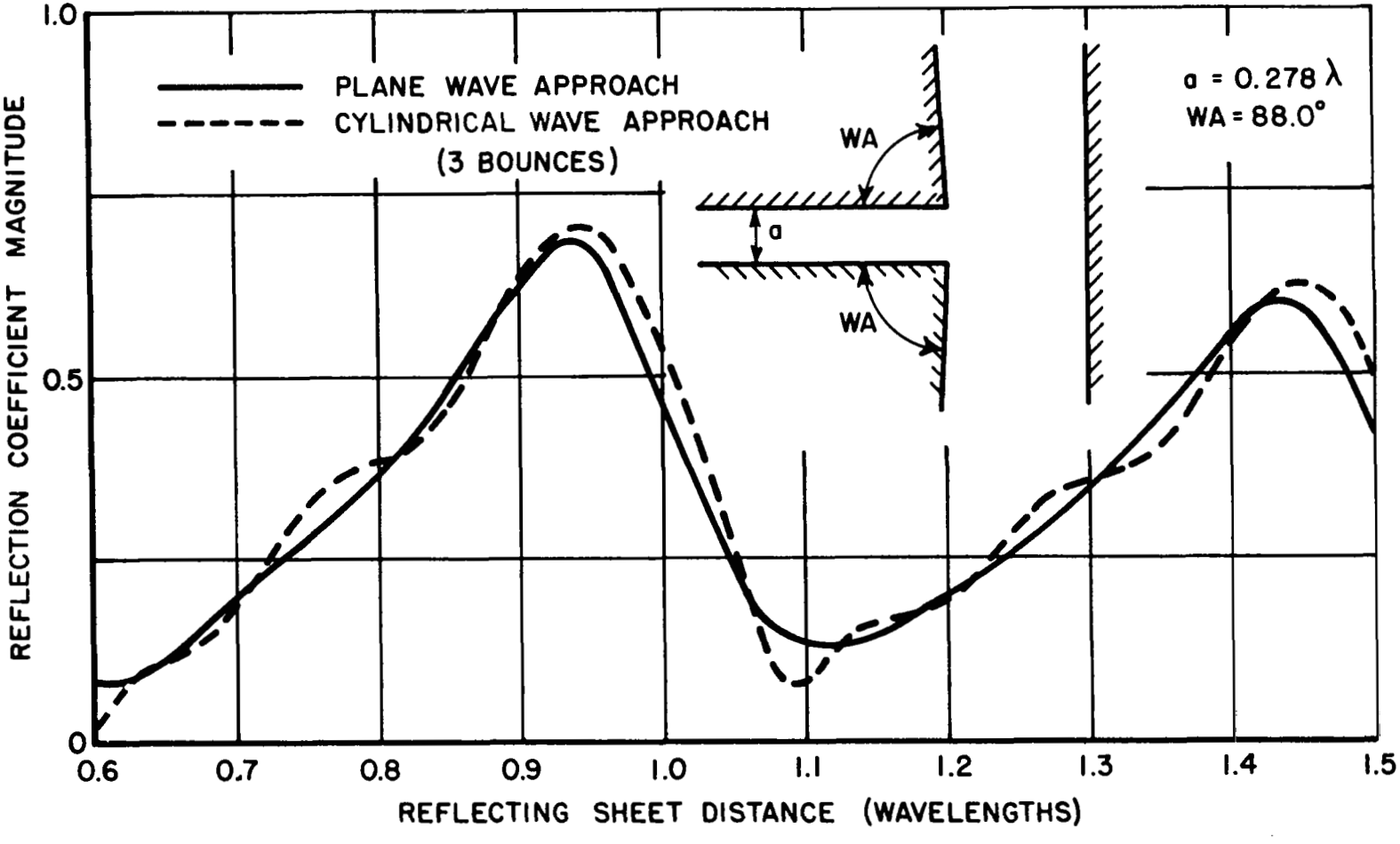

Fig. 24. Comparison of the reflection coefficient magnitude (a = 0. 278λ, WA = 88°).

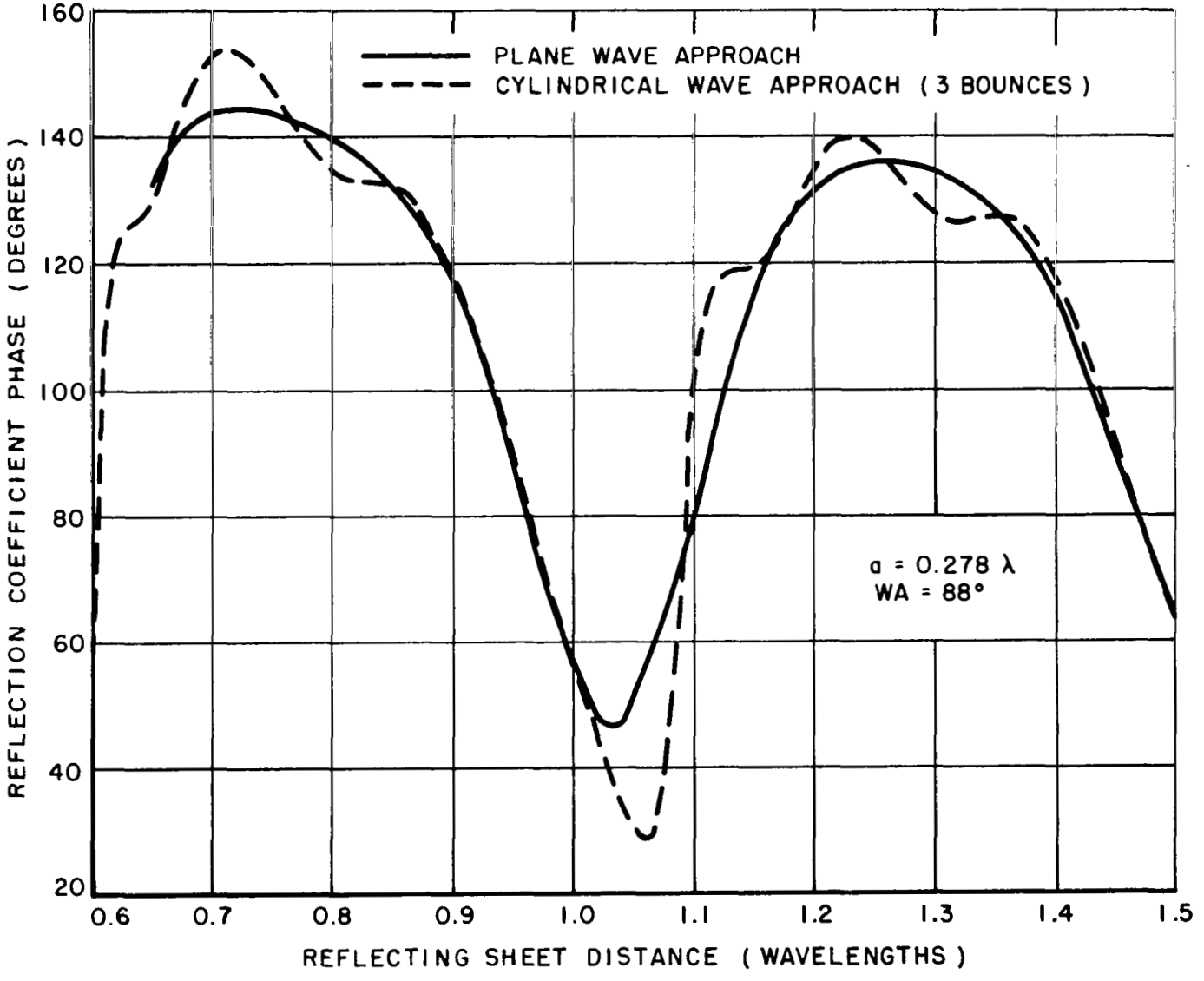

Fig. 25. Comparison of the reflection coefficient phase (a = 0. 278λ, WA = 88°).

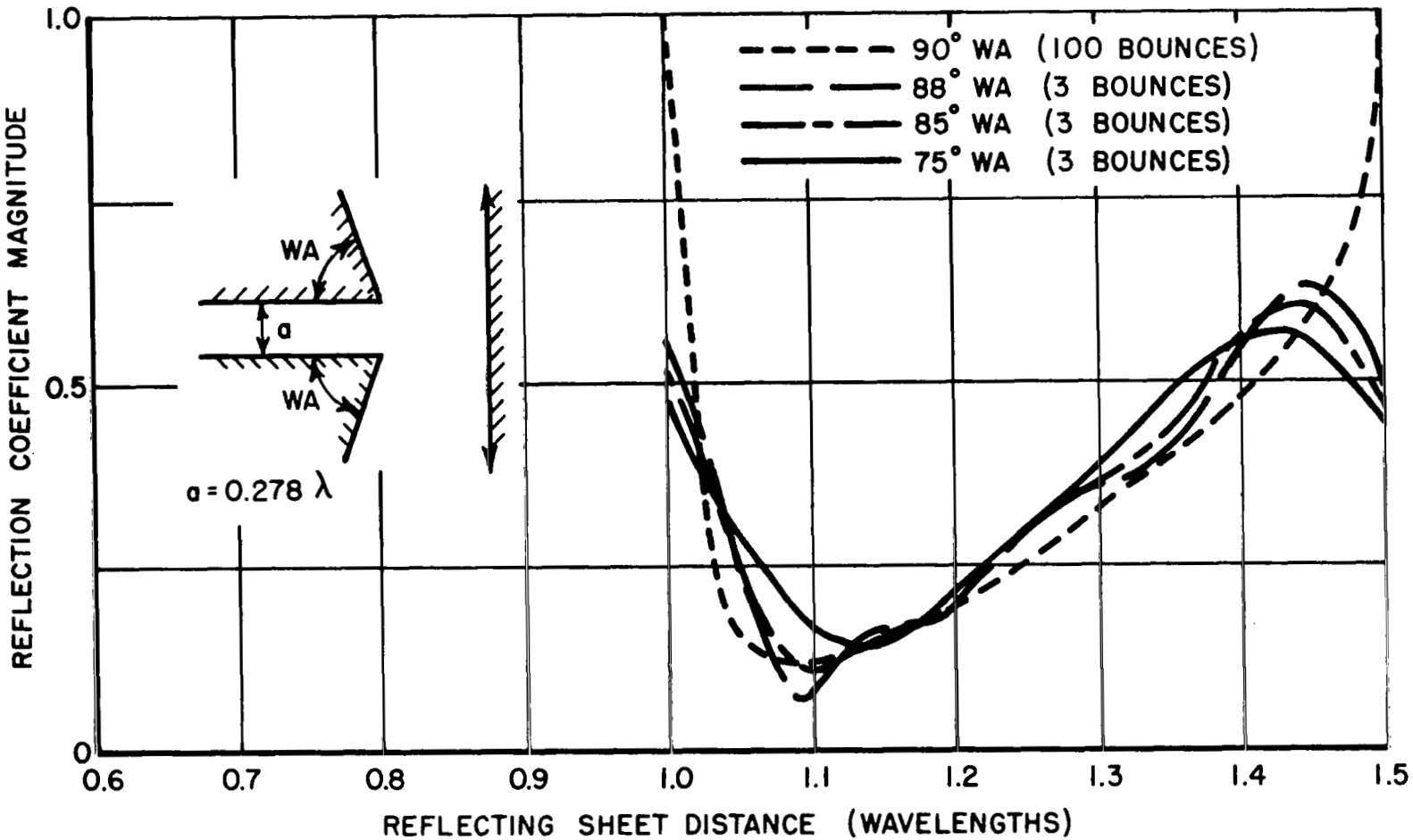

Fig. 26. The reflection coefficient magnitude calculated by the cylindrical wave approach shown as a function of wedge angles.

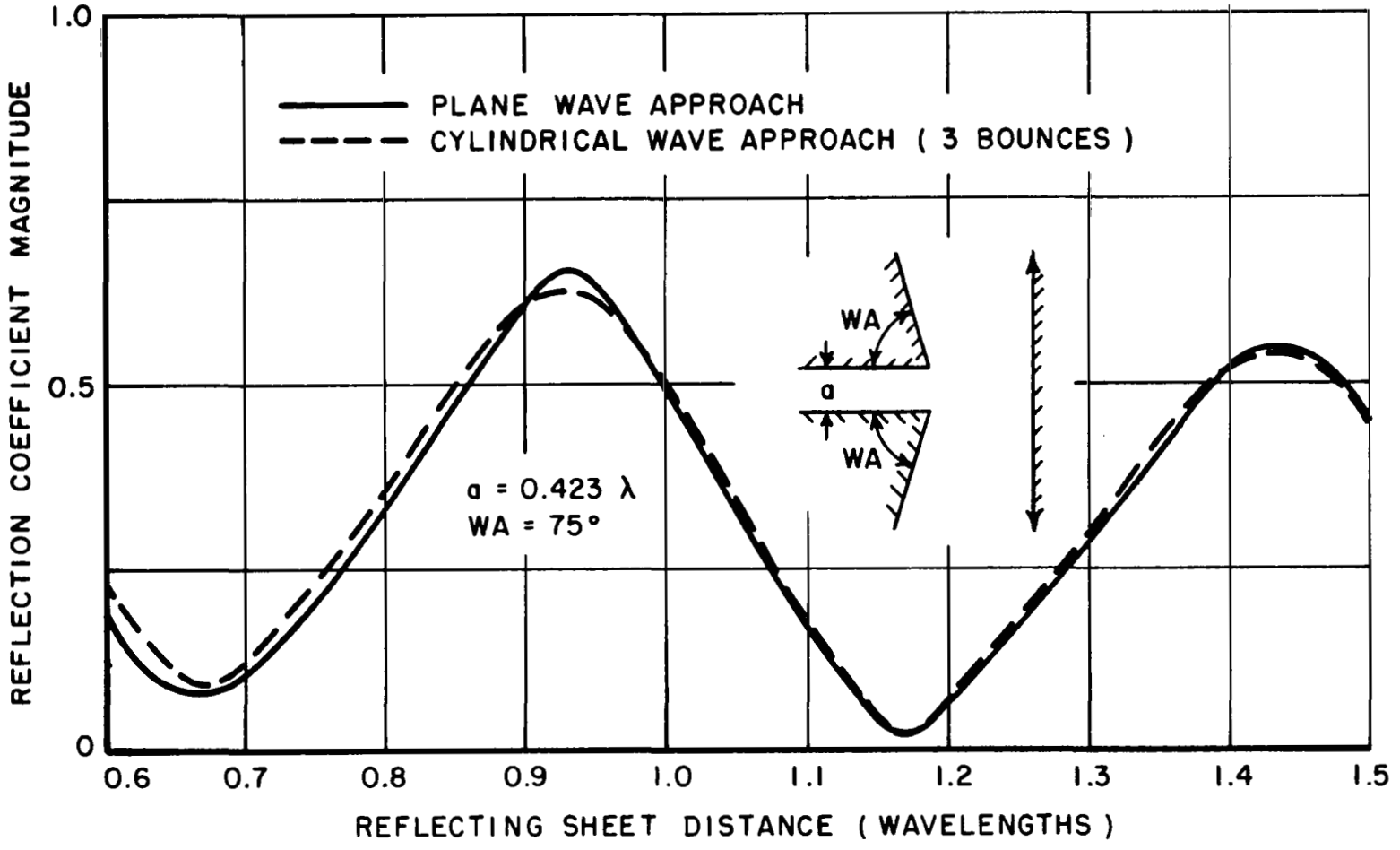

Fig. 27. Comparison of reflection coefficient magnitude (a = 0. 423λ, WA = 75°).

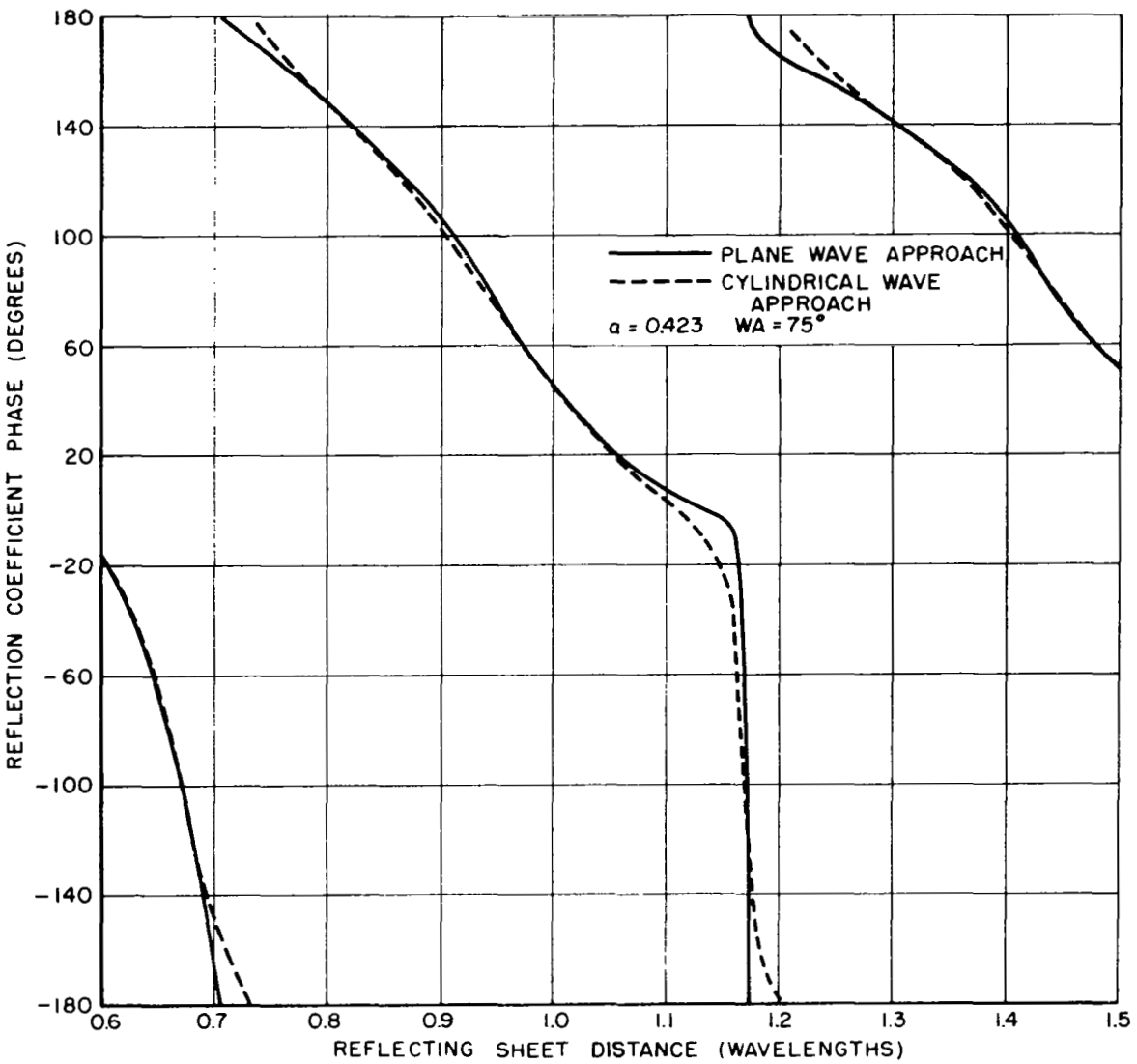

Fig. 28. Comparison of reflection coefficient phase ($a = 0.423\lambda$, $WA = 75°$).

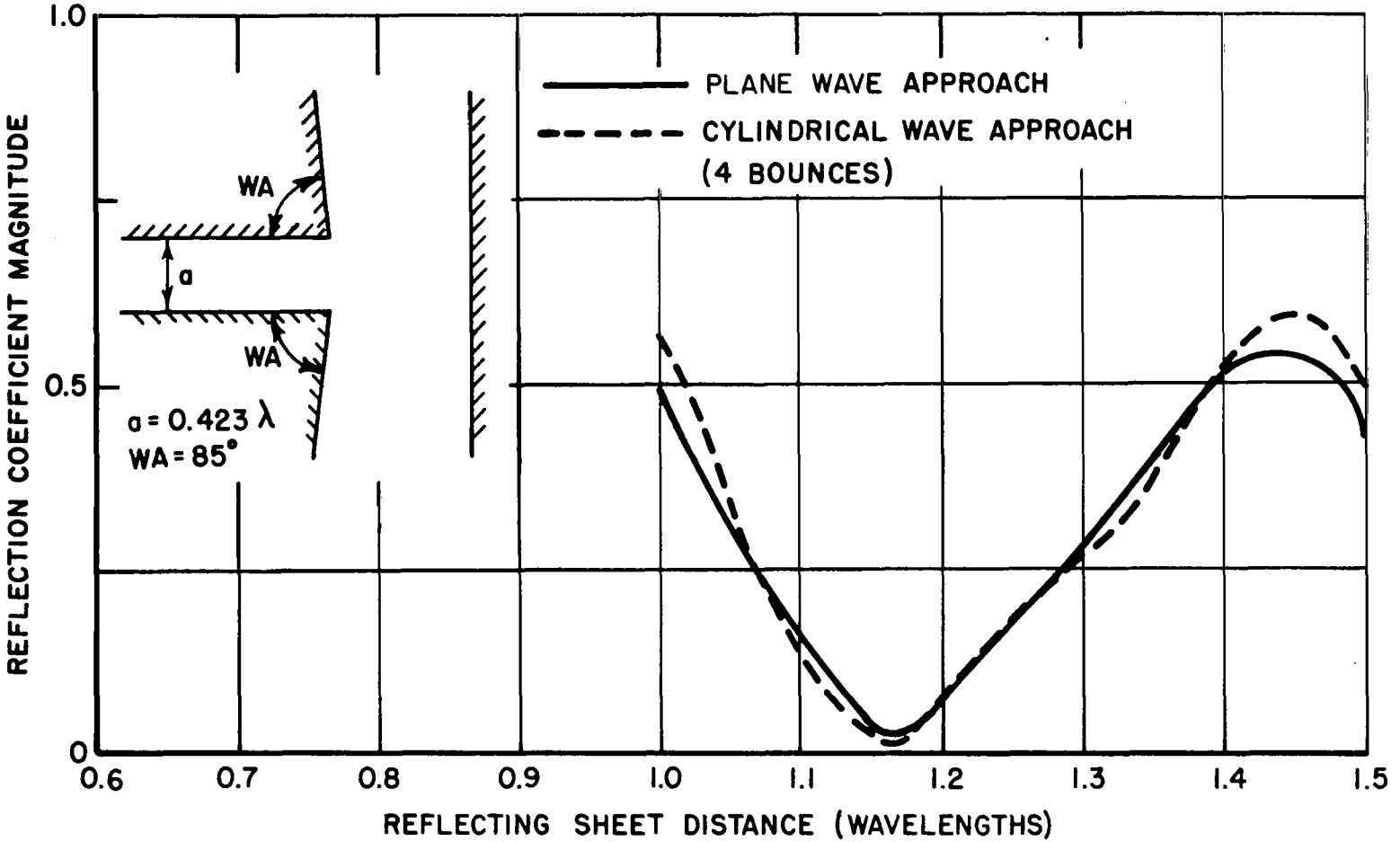

Fig. 29. Comparison of reflection coefficient magnitude (a = 0. 423λ, WA = 85°).

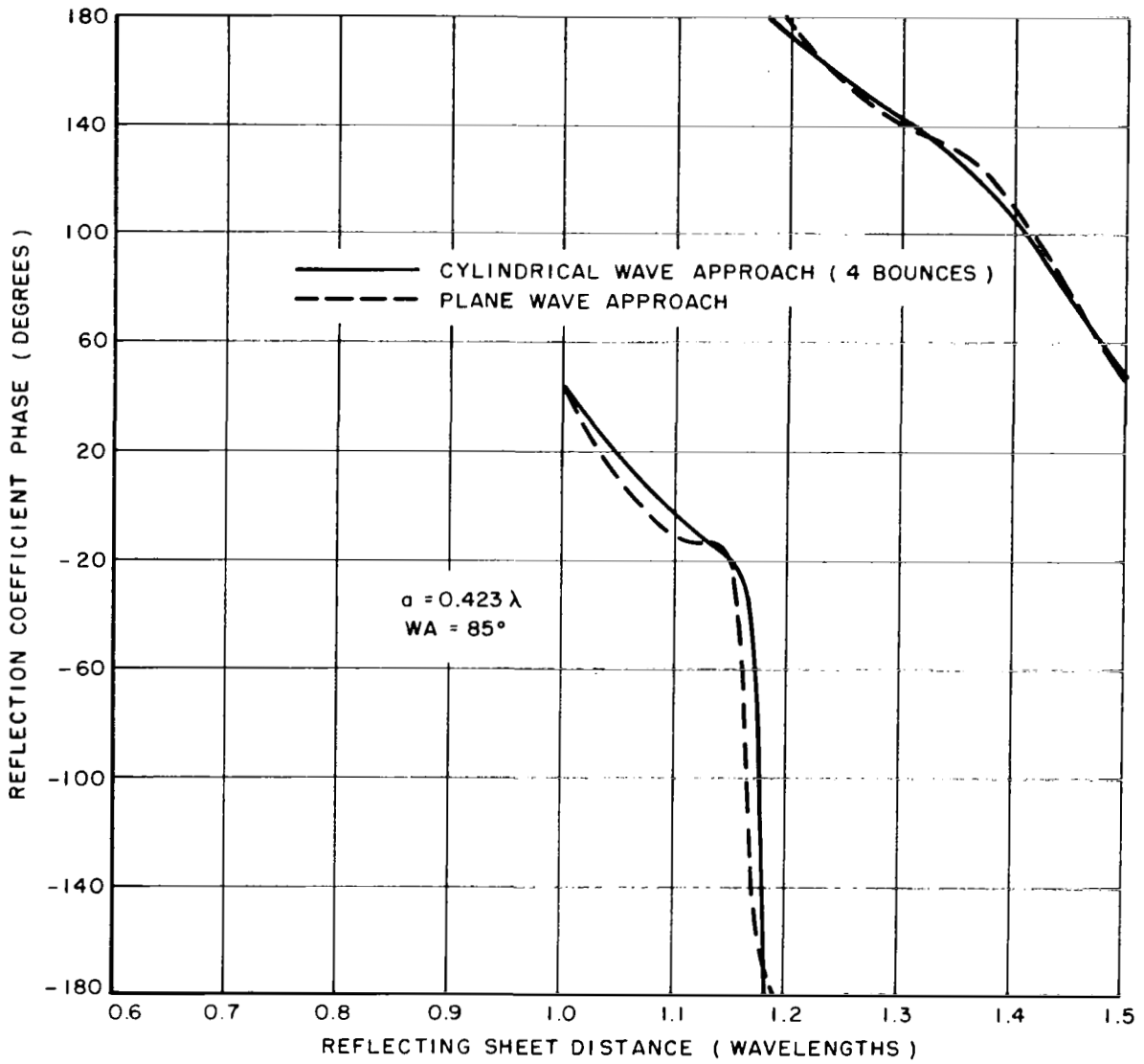

Fig. 30. Comparison of reflection coefficient phase ($a = 0.423\lambda$, WA = 85°).

V. CONCLUSIONS

The reflection coefficient for the large wedge angle parallel-plate waveguide operating in the TEM mode and illuminating a perfectly reflecting sheet was analyzed by wedge diffraction techniques. With this analysis and those in References 1 and 2 a complete coverage of wedge angles is achieved.

Good agreement is obtained between the results calculated by the cylindrical wave method of this report and the plane wave method of Reference 1 in their mutual regions of validity; i. e. , at wedge angles from 0° to 80°. Good agreement is also obtained with measurements.

Computations made from this analysis indicate that the plane-wave approach is useful for wedge angles as large as 85°. In fact a major contribution of this cylindrical-wave analysis is to check the validity of the plane-wave approach.

Based on the bounce analysis the reflection coefficient is seen to converge more rapidly as a function of the number of bounces included when the wedge angle decreases. In fact, for the 75° wedge angle case only three bounces are required.

REFERENCES

1. Tsai, L. L., "The Reflection Coefficient of a TEM Model Parallel-Plate Waveguide Illuminating a Perfectly Reflecting Sheet," Report 2143-1, 25 August 1966, ElectroScience Laboratory, The Ohio State University; prepared under Grant NGR-36-008-048, National Aeronautics and Space Administration, Office of Grants and Research Contracts, Washington, D. C.

2. Tsai, L. L. and Rudduck, R. C., "The Reflection Coefficient of a Ground-Plane Mounted TEM Model Parallel-Plate Waveguide Illuminating a Conducting Sheet," (in preparation).

3. Rudduck, R. C., "Application of Wedge Diffraction to Antenna Theory," Report 1691-13, 30 June 1965, ElectroScience Laboratory, The Ohio State University Research Foundation; prepared under Grant NsG-448, National Aeronautics and Space Administration, Office of Grants and Research Contracts, Washington, D. C.

4. Dybdal, R. B., Rudduck, R. C. and Tsai, L. L., "Mutual Coupling Between TEM and TE_{01} Parallel-Plate Waveguide Apertures," IEEE Transactions on Antennas and Propagation, Vol. AP-14, No. 5, September 1966, pp. 574-580.

5. Rudduck, R. C. and Tsai, L. L., "Aperture Reflection Coefficient of TEM and TE_{01} Mode Parallel-Plate Waveguides," to be published in the January 1968 issue of the IEEE Transactions on Antennas and Propagation.

"The aeronautical and space activities of the United States shall be conducted so as to contribute . . . to the expansion of human knowledge of phenomena in the atmosphere and space. The Administration shall provide for the widest practicable and appropriate dissemination of information concerning its activities and the results thereof."

—NATIONAL AERONAUTICS AND SPACE ACT OF 1958

NASA SCIENTIFIC AND TECHNICAL PUBLICATIONS

TECHNICAL REPORTS: Scientific and technical information considered important, complete, and a lasting contribution to existing knowledge.

TECHNICAL NOTES: Information less broad in scope but nevertheless of importance as a contribution to existing knowledge.

TECHNICAL MEMORANDUMS: Information receiving limited distribution because of preliminary data, security classification, or other reasons.

CONTRACTOR REPORTS: Scientific and technical information generated under a NASA contract or grant and considered an important contribution to existing knowledge.

TECHNICAL TRANSLATIONS: Information published in a foreign language considered to merit NASA distribution in English.

SPECIAL PUBLICATIONS: Information derived from or of value to NASA activities. Publications include conference proceedings, monographs, data compilations, handbooks, sourcebooks, and special bibliographies.

TECHNOLOGY UTILIZATION PUBLICATIONS: Information on technology used by NASA that may be of particular interest in commercial and other non-aerospace applications. Publications include Tech Briefs, Technology Utilization Reports and Notes, and Technology Surveys.

Details on the availability of these publications may be obtained from:

SCIENTIFIC AND TECHNICAL INFORMATION DIVISION

NATIONAL AERONAUTICS AND SPACE ADMINISTRATION

Washington, D.C. 20546